Climate Dynamics (2021) 56:3005–3024
https://doi.org/10.1007/s00382-021-05627-w

Changes in the equatorial mode of the Tropical Atlantic in terms of the Bjerknes Feedback Index

Paulo Silva[1] · **Ilana Wainer**[1] · **Myriam Khodri**[2]

Received: 20 January 2020 / Accepted: 2 January 2021 / Published online: 13 January 2021

Abstract
One of the main modes of sea surface temperature variability in the Tropical Atlantic is the Atlantic Equatorial Mode or Atlantic Niño. The region of largest interannual variability, where the Atlantic Cold Tongue forms, is also a region of consistent biases in climate models. In this study, we investigate the interannual variability of the Tropical Atlantic and its changes in the recent decades in terms of the Bjerknes Feedback Index (I_{BJ}) in a set of seven ocean reanalyses for the periods 1980–1999 and 2000–2010. Differences were observed among the reanalyses regarding their representation of each term of the Bjerknes Feedback, particularly regarding zonal surface currents, leading to differences in dynamical damping and the zonal advective feedback. However, a consistent negative index (damped) is observed in all reanalysis, with the thermocline feedback being the dominant positive term and thermal damping the dominant negative term. Warming trends are observed in sea surface temperatures in the cold tongue region in all reanalyses, as well as a decrease in interannual variability. These in turn are associated with a weakening in the Bjerknes Feedback in the early XXI century, indicated by a stronger and negative index. This results from a stronger thermal damping and weaker thermocline feedback, associated with a weaker response of equatorial zonal thermocline slope to equatorial zonal wind stress. Despite the spread among the reanalysis, the results obtained are consistent with previous studies.

Keywords Bjerknes Feedback · Equatorial Atlantic · Ocean reanalysis · Tropical variability

1 Introduction

The study of sea surface temperature (SST) variability is important because of its strong influence on precipitation and the consequent social and economic impacts (Lübbecke and McPhaden 2013). Of particular interest is SST variability in the Tropical Atlantic due to its influence on the climate of the surrounding continents. Recurrent patterns of SST and wind anomalies in this region are linked to the intensity of the West African Monsoon and the distribution of rainfall in Northeast Brazil (Xie and Carton 2013; Brierley and Wainer 2018). A principal means by which this happens is through the effect of SST on sea level pressure and, consequently, on wind patterns and the position of the Intertropical Convergence Zone (ITCZ) (Lindzen and Nigam 1987; Carton et al. 1996; Back and Bretherton 2009a, b). Variability in this region, particularly off the Central African Coast , has also been shown to impact this region's marine ecosystems, specifically affecting local fish availability (Binet et al. 2001).

The mean annual cycle is responsible for the greatest share of variability in the Tropical Atlantic Ocean (Carton and Zhou 1997; Xie and Carton 2013). The mean annual SSTs and wind stress are shown Fig. 1a and the mean thermocline depth and surface currents, in Fig. 1b, obtained from the Ocean ReAnalysis System 4 (ORAS4 Balmaseda et al. 2013). The ITCZ can be observed slightly north of the equator, where the southeasterly and northeasterly trade winds converge in a zone of warmest SSTs around 5°N. As a result of the predominantly zonal and westward wind stress, the thermocline is shallower in the east and deeper in the west.

✉ Paulo Silva
paulo2.silva@usp.br

Ilana Wainer
wainer@usp.br

Myriam Khodri
myriam.khodri@locean-ipsl.upmc.fr

[1] Oceanographic Institute, University of São Paulo, Praca do Oceanografico 191, São Paulo, SP 05508120S, Brazil

[2] LOCEAN-IRD/IPSL, Sorbonne University, Paris, France

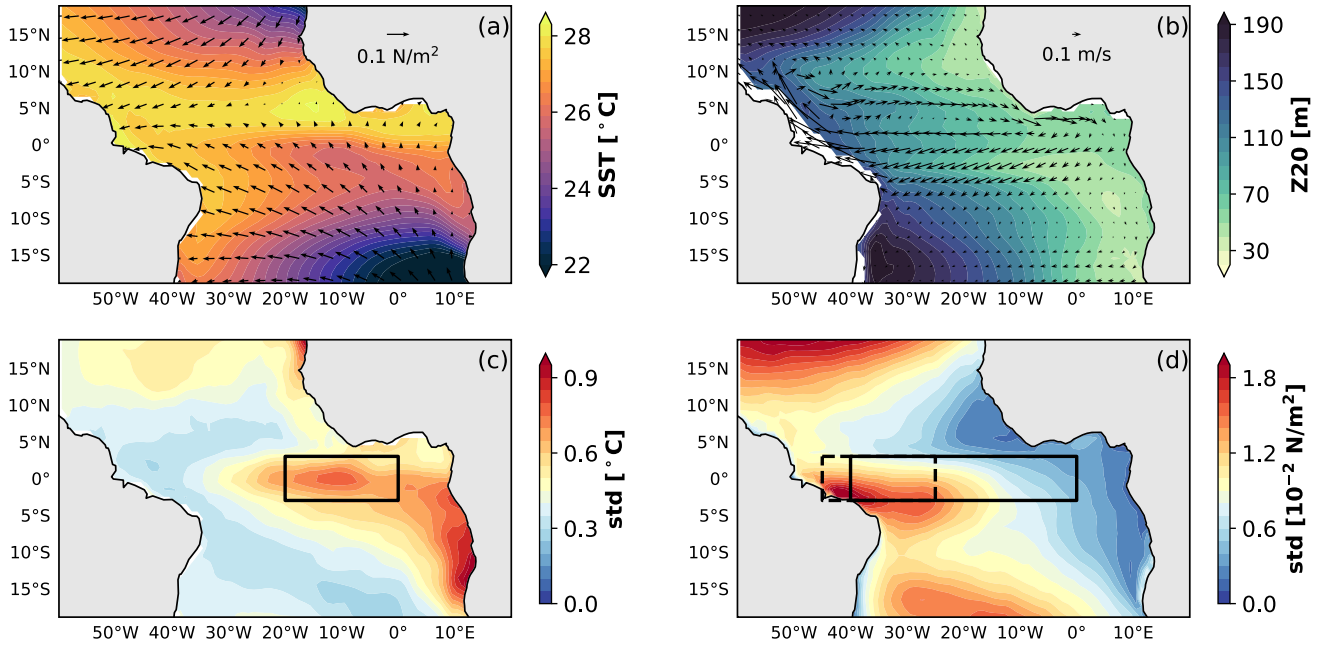

Fig. 1 **a** Mean SST (°C) and wind stress (N/m^2) and **b** mean thermocline depth (m), considered as the depth of the 20°C isotherm (Z20) and mean surface (35 m) currents (m/s); **c** JJA standard deviation of SST and ATL3 region (3°N–3°S; 20°W–0°), which is used as the index region of the equatorial mode; **d** MAM standard deviation of zonal wind stress and WATL (3°N–3°S; 45°W–25°W, dashed line) and mean equatorial region (3°N–3°S; 40°W–0°, solid line), used in the computation of the Bjerknes Feedback Index

The fact that the ITCZ shifts northward throughout the year and that the southern trades cross the equator, varying in strength throughout the year, have important implications for the annual cycle of equatorial SSTs (Xie 1994). In austral autumn (MAM), temperatures are highest in the equatorial region, sometimes exceeding 27 °C, since the Sun is at its highest position at this time of the year. In this period, the ITCZ is located nearly on the equator. Because the ITCZ is characterized by calm winds, the easterly winds that cause the equatorial thermocline to be deeper in the west and shallower in the east weaken and, as a result, the eastern thermocline deepens and the western one shoals, decreasing the equatorial thermocline slope. The trades then intensify in austral winter (JJA), resulting in increased upwelling in the east. The stronger trades also play a role in the shoaling of the thermocline in the east, although a large part of this shoaling is associated with the propagation of equatorial Kelvin waves (Ding et al. 2009). The shoaling thermocline leads to lower SSTs forming the equatorial Atlantic Cold Tongue (ACT) in the eastern equatorial region and along the southwestern African coast. The formation of the cold tongue can be related to the onset of the West African Monsoon, through the intensification of the land–ocean pressure gradient (Okumura and Xie 2004; Xie and Carton 2013).

In addition to the annual cycle, there is also interannual variability in the Tropical Atlantic. The physical mechanisms of air-sea interaction that occur in this region resemble those that give rise to the El Niño–Southern Oscillation (ENSO) in the Pacific, resulting in similar patterns of variability (Zebiak 1993). This variability is represented by two leading SST modes: the Atlantic Equatorial Mode, also referred to as the Atlantic Niño, and the Atlantic Meridional Mode, with generally opposite north and south polarities about the equator (Chiang and Vimont 2004; Brierley and Wainer 2018). The equatorial and meridional modes correspond to the two first empirical orthogonal functions (EOFs) of detrended monthly tropical Atlantic SST anomalies (Deser et al. 2010). The relative importance of both modes is similar, so that different studies suggest different leading modes (e.g., Servain et al. 2003; Amaya et al. 2017).

In this study we focus on the Atlantic equatorial mode. This mode is related to the interannual variability of the ACT, which is the region of highest interannual SST variability in JJA (Fig. 1c); the variability of equatorial winds lead that of SST in the ACT region, peaking in MAM (Richter et al. 2013) (Fig. 1d). Much like the Pacific El Niño, the Atlantic equatorial mode is characterized by the coupling between SST anomalies in the cold tongue region, zonal wind anomalies and consequent thermocline depth and upwelling anomalies, known as the Bjerknes Feedback (Bjerknes 1969; Keenlyside and Latif 2007; Deppenmeier et al. 2016; Dippe et al. 2019). However, unlike the case of the Pacific, interannual variability of the Atlantic equatorial mode has been suggested by Burls et al. (2012) to be a modulation of the seasonal cycle, which is more pronounced in this region; likewise, it has been shown by Prodhomme et al.

(2019) that the ability of coupled models to reproduce equatorial Atlantic interannual variability is tied to their ability of realistically reproducing its seasonal cycle. In addition, the Atlantic equatorial mode is more concentrated at the equator and displaced farther east in the basin than the Pacific mode (Zebiak 1993). It is also weaker than its Pacific counterpart with frequencies of 2–4 years (Zebiak 1993; Servain et al. 1999; Deser et al. 2010). Its periodicity also varies considerably (Xie and Carton 2013). Nonetheless, its signal is robust, as demonstrated by e.g. Keenlyside and Latif (2007).

As stated by Losada et al. (2010), the Atlantic equatorial mode is strongly coupled to West African rainfall variability. The authors show that an anomalous warming in the equatorial Atlantic in Austral winter results in a weakening of the West African Monsoon by diminishing the sea level pressure gradient between the equator and the Saharan heat low. On the same note, Tokinaga and Xie (2011) show how the decrease in cold tongue SST variability in the past decades is associated with a decrease in rainfall variability over the coast of Guinea. The equatorial mode has also been shown to have teleconnections with the extratropical atmosphere and the North Atlantic circulation through the impact of cold tongue anomalies on the Hadley circulation and the northern subtropical jet (Haarsma and Hazeleger 2007) and to affect the Indian summer monsoon through perturbations in the Asian subtropical jet (Kucharski et al. 2007, 2008; Yadav et al. 2018).

However, despite the rapid progress made in the last decades in understanding these mechanisms, global climate models are known to show large biases in the Equatorial Atlantic (Richter and Xie 2008; Richter et al. 2012, 2014; Deppenmeier et al. 2016; Zuidema et al. 2017). In addition, observational data in the Tropical Atlantic tends to be more sparse than in the Tropical Pacific and Indian Oceans (Xue et al. 2012) and differences among ocean reanalyses that assimilate this data using different models and assimilation methods give rise to differences among these products that are comparable to or larger than interannual variability in the region (Zhu et al. 2012). Contrasting results have been obtained in studies regarding the variability of the equatorial Atlantic as well; Tokinaga and Xie (2011) found from observational data a weakening in ACT variability during 1950–2009, associated with a warming of the eastern equatorial Atlantic (hereafter EEA), weaker trades and a deeper thermocline in the east; Servain et al. (2014), on the other hand, found a strengthening in the trades in 1964–2012 despite the warming in the EEA, also using observations; more recently, Nnamchi et al. (2020) report that despite the warming elsewhere in the tropical Atlantic, there is a 'warming hole' in the cold tongue region in the satellite era (1978–2018), driven by increased wind stress forcing and a shallower eastern thermocline. With this in mind, this study aims to investigate the Equatorial Atlantic variability in the period 1980–2010 and assess the robustness of the Bjerknes Feedback across seven reanalysis products in the Atlantic, as well as potential changes in this feedback after 2000, in terms of the Bjerknes Feedback Index (Jin et al. 2006).

2 Methods

The growth of ENSO-related SST anomalies in the Pacific and the transition from the warm to cold phase of its equatorial mode were explained by Jin (1997) and Jin and An (1999) in terms of an oscillator model of recharge and discharge of equatorial heat content. As discussed by e.g. Jansen et al. (2009); Ding et al. (2010), the same framework can be applied to the Atlantic equatorial mode, since the underlying dynamics is similar.

In this model, the Bjerknes Feedback is composed of different components and damping mechanisms (Fig. 2) that enhance and limit the growth of the SST anomalies. In the warm phase, an initial positive SST anomaly in the east leads to the weakening of the trade winds by decreasing the surface zonal pressure gradient. The westerly wind anomaly forcing diminishes the zonal thermocline slope, by making it shallower in the west and deeper in the east. It also generates an anomalous eastward zonal current. In addition, upwelling in EEA is reduced as a response to the weaker trades. The opposite effect is observed in the cold phase, that is, a negative SST anomaly in the east leads to a strengthening of the trade winds, a shoaling of the eastern thermocline and consequent increased upwelling in EEA. Therefore, the combined effect of the anomalous thermocline depth, zonal current and upwelling results in the increase of the initial SST anomaly. These are called, respectively, the *thermocline, zonal advective* and *Ekman feedbacks* (hereafter TF, ZAF and EF). The further growth of the anomaly is limited by *thermal* and *dynamical damping* (hereafter TD and DD), which are related to the net surface heat flux (NSHF) and the effect of the mean (climatological) currents, respectively.

The Bjerknes feedback index (hereafter I_{BJ}) was derived by Jin et al. (2006) from the linear equation of SST anomalies in the mixed layer averaged over the eastern equatorial Pacific. According to their derivation, the time derivative of the SST anomalies is proportional to the I_{BJ} and the anomaly, as show in Eq. 1.

$$\frac{\partial \tilde{T}}{\partial t} = 2I_{BJ}\tilde{T} + F[h] \tag{1}$$

where $\tilde{T}$ represents the SST anomaly and the term $F[h]$ is related to heat content recharge/discharge in the transition between the positive and negative phases. The I_{BJ} has dimension of time^{-1} and measures the growth rate of SST anomalies associated with the Bjerknes feedback, as follows. If

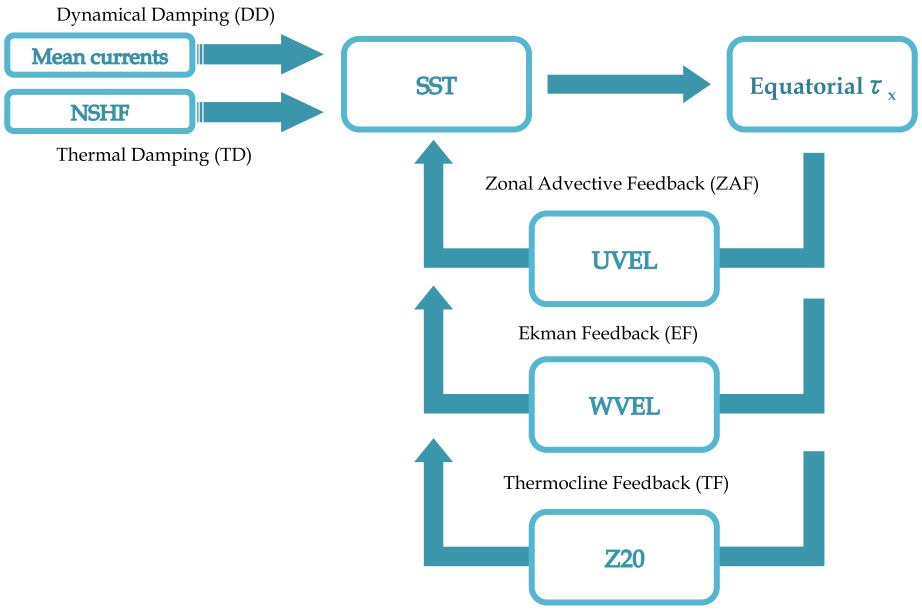

Fig. 2 Schematic representation of the Bjerknes Feedback and its components: an initial SST anomaly in the eastern equatorial Atlantic (EEA) leads to anomalies in equatorial zonal wind stress, which in turn leads to anomalies in the zonal currents (ZAF), upwelling (EF) and thermocline depth (TF), ultimately resulting in the amplification of the initial anomaly. SST anomalies growth is limited by the effect of the mean (climatological) currents (DD) and anomalous net surface heat flux (TD). NHSF, UVEL, WVEL and Z20 stand for net surface heat flux, zonal current velocity, vertical current velocity and thermocline depth considered as the depth of the 20 °C isotherm, respectively

the I_{BJ} is negative and the anomaly is positive, the anomaly derivative will be negative; likewise, if the anomaly is negative, its derivative will be positive. This means that a negative I_{BJ} weakens the initial SST anomaly. The opposite happens if I_{BJ} is positive. Therefore, a positive I_{BJ} indicates an unstable coupled system, with anomalies growing exponentially, while negative values indicate the anomaly's growth is limited. Both the Atlantic and the Pacific equatorial modes are damped, although damping is stronger in the Atlantic (Lübbecke and McPhaden 2013). The I_{BJ} takes its negative contributions from TD and DD and positive contributions from ZAF, EF and TF, as shown in Eq. 2:

$$2I_{BJ} = \underbrace{-\left(\frac{\langle\bar{u}\rangle_{ATL3}}{L_x} + \frac{\langle -2y\bar{v}\rangle_{ATL3}}{L_y^2} + \frac{\langle\bar{w}\rangle_{ATL3}}{H_m}\right)}_{\mathrm{DD}}\overbrace{-\alpha}^{\mathrm{TD}} \underbrace{+\mu_a\beta_u\left\langle\frac{-\partial\bar{T}}{\partial x}\right\rangle_{ATL3}}_{\mathrm{ZAF}} \underbrace{+\mu_a\beta_w\left\langle\frac{-\partial\bar{T}}{\partial z}\right\rangle_{ATL3}}_{\mathrm{EF}} \underbrace{+\mu_a\beta_h\left\langle\frac{H(\bar{w})\bar{w}}{H_m}a_h\right\rangle_{ATL3}}_{\mathrm{TF}} \tag{2}$$

In Eq. 2, T represents temperature; u,v and w represent zonal, meridional and vertical velocities; L_x and L_y stand for the zonal and meridional extent of the averaging region and y, the distance from the equator; the overbar denotes climatological mean; and $\langle\rangle_{ATL3}$ denotes the volume average over the region of highest SST variability, which corresponds to the ATL3 region (Fig. 1c) in the Tropical Atlantic, and from the surface to the mixed layer depth. Here the mixed layer depth used as the lower boundary is the climatological mean. H_m is the effective depth for vertical advection, which is the first vertical level showing high vertical velocities. It is obtained by computing the mean vertical velocity profile in the ATL3

region and picking the level where vertical velocity peaks. $H()$ is the Heaviside function, so that $H(\bar{w})\bar{w}$ represents upwelling by excluding negative values from the vertical velocity field.

The parameters α, μ_a, β_u, β_w, β_h and a_h are obtained through linear regression between the detrended anomaly series of the corresponding variables.

The term α represents the thermal damping of SST anomalies and is obtained through the linear regression of mean SST anomalies in the ATL3 region and NSHF anomalies averaged in the same region, according to Eq. 3, where the tilde indicates the monthly anomaly of the variable is being considered:

$$\left\langle \tilde{Q}_{net} \right\rangle_{ATL3} = \alpha \left\langle \tilde{T} \right\rangle_{ATL3} \tag{3}$$

The parameter μ_a represents the response of equatorial zonal wind stress to SST anomalies in the east and is obtained by regressing the mean equatorial zonal wind stress (solid line region in Fig. 1d and indicated by [ ] in the equation) onto ATL3 SST anomalies (Eq. 4).

$$[\tilde{\tau}_x] = \mu_a \left\langle \tilde{T} \right\rangle_{ATL3} \tag{4}$$

The parameter β_u represents the response of zonal current anomalies in the EEA to anomalous equatorial wind stress and is the first coefficient of the multilinear regression between zonal current anomalies and zonal wind stress and western thermocline slope anomalies (Eq. 5).

$$\langle \tilde{u} \rangle_{ATL3} = \beta_u [\tilde{\tau}_x] + \beta_{uh} \left\langle \tilde{Z20} \right\rangle_{WATL} \tag{5}$$

where $\langle\rangle_{WATL}$ represents the volume average over the WATL region in the west equatorial Atlantic (Fig. 1d) and from the surface to the mixed layer depth and β_{uh} represents the adjustment of the zonal current anomalies to the thermocline.

The term β_w represents the response of upwelling in the ATL3 region to anomalous equatorial wind stress and is obtained from the linear regression of ATL3 upwelling anomalies and equatorial zonal wind stress anomalies (Eq. 6).

$$\langle H(\bar{w})\tilde{w} \rangle_{ATL3} = -\beta_w [\tilde{\tau}_x] \tag{6}$$

The parameter β_h is obtained from the regression between equatorial zonal wind stress anomalies and the zonal thermocline slope (Eq. 7). Here thermocline slope is defined as the difference between thermocline depth in ATL3 and WATL, so that a positive anomaly in thermocline slope indicates the eastern thermocline is deeper (positive anomaly in the east) and the western is shallower (negative anomaly). In this case, the zonal thermocline slope is reduced. Likewise, a negative thermocline slope anomaly indicates the zonal slope is steeper.

$$\left\langle \tilde{Z20} \right\rangle_{ATL3} - \left\langle \tilde{Z20} \right\rangle_{WATL} = \beta_h [\tilde{\tau}_x] \tag{7}$$

Finally, a_h is obtained from the regression between ATL3 thermocline depth anomalies and anomalous subsurface temperatures in this region, according to Eq. 8. $\tilde{T}_{sub}$ is the mean anomalous temperature, which is averaged from the surface to the thermocline, using a time-varying thermocline depth. $\tilde{T}_{sub}$ is multiplied by $\langle H(\bar{w}) \rangle_{ATL3}$, so that only upwelling is taken into consideration.

$$\left\langle H(\bar{w})\tilde{T}_{sub} \right\rangle_{ATL3} = a_h \left\langle \tilde{Z20} \right\rangle_{ATL3} \tag{8}$$

The error margins are calculated for the dynamical damping terms based on the standard error (standard deviation divided by the square root of the number of observations) of the mean currents in the ATL3 region averaged from the surface to the mean mixed layer depth. For example, if the mixed layer extends from the surface to the seventh vertical level, the standard error of the mean zonal current is the standard deviation of the mean ATL3 zonal currents in each of the seven vertical levels, divided by $\sqrt{7}$. The same applies to the remaining terms in brackets in Eq. 2. The error of the regression parameters obtained in Eqs. 3–8 are the standard errors of the regression slopes, obtained from Eq. 9:

$$SE = \sqrt{\frac{1}{n-2} \frac{\sum (y_i - \hat{y}_i)^2}{\sum (x_i - \bar{x})^2}} \tag{9}$$

where n is the number of observations, $\hat{y}_i$ are the estimated values of the dependent variable and $\bar{x}$ is the mean of the observed values of the independent variable. The total errors of each feedback term as well as the error of the total index are obtained through the error propagation formulas. This is done for each individual reanalysis product used. The standard errors associated with the reanalyses ensemble means are calculated by dividing the ensemble standard deviations by the square root of the number of ensemble members (7).

3 Data

Monthly means from seven oceanic reanalyses (Table 1) from the Ocean Reanalysis Intercomparison Project (ORA-IP) (Balmaseda et al. 2015) are used for the period spanning from 1980 to 2010, in which all reanalysis overlap. To allow comparison, all products were interpolated to a 1° horizontal resolution and 40 vertical levels, which is the coarser resolution among them. As vertical velocity is only available for CFSR and GECCO2, it is estimated for the other reanalysis from the continuity equation using the horizontal velocity fields, integrating from the bottom up. The 20 °C isotherm depth (Z20) is chosen as a proxy for thermocline depth as it usually is located near the center of the thermocline in the

Table 1 Summary of the ocean reanalysis products used

Reanalysis	Model	Assimilation method	Resolution	Reference
CFSR NOAA/NCEP	MOM4	3DVAR	0.5° × 0.5°, 40 levels	Saha et al. (2010)
ECDA v.3 NOAA/GFDL	MOM4	Ensemble Kalman Filter	1° × 1/3°, 50 levels	Zhang et al. (2007)
GECCO2 U. Hamburg	MITgcm	4DVAR	1° × 1/3°, 50 levels	Köhl (2015)
GODAS NOAA/NCEP	MOM3	3DVAR	1° × 1/3°, 40 levels	Behringer (2007)
K7-ODA JAMSTEC	MOM3	4DVAR	1° × 1°, 46 levels	Masuda et al. (2010)
ORAS4 ECMWF	NEMO3	3DVAR	1° × 1°, 42 levels	Balmaseda et al. (2013)
SODA v.3.4.1 U. Maryland and TAMU	MOM5	Optimal interpolation	0.25° × 0.4°, 50 levels	Carton et al. (2018)

equatorial oceans (Yang and Wang 2009). The mixed layer depth is taken as 35 m for all reanalyses, based on their mean temperature profile in the ATL3 region across the period analyzed. In addition to the seven oceanic reanalyses, one product of bias-corrected net surface heat flux for the tropical regions (TropFlux) is used (Kumar et al. 2012).

4 Results

In Sect. 4.1 we investigate the strength of the Bjerknes Feedback in each reanalysis product in terms of the I_{BJ} computed for the whole period they have in common (1980–2010). Then, in Sect. 4.2, we investigate the changes in the Bjerknes feedback before and after 2000 using the I_{BJ}.

4.1 Bjerknes Feedback Index

Dynamical damping (DD) In EEA, the mean zonal currents are westward, the mean meridional currents are diverging and the mean vertical velocity is upward as shown in e.g. Stramma and Schott (1999) and Fig. 1b. Westward currents act to enhance SST anomalies, as do mean downward vertical velocities and meridional velocities directed away from the anomaly; Therefore, the zonal, meridional and vertical contributions to the dynamical damping term are expected to be positive, negative and negative, respectively. Likewise, mean eastward zonal currents, upward vertical currents and converging meridional currents would have the opposite effect.

The dynamical dampings obtained for each reanalysis are shown in Table 2. All terms are computed based on the average of the mean currents in the ATL3 region and from the surface to the mixed layer depth. Although the ultimate effect of the mean currents is to damp the anomalies,

Table 2 Zonal (DD_u), meridional (DD_v), vertical (DD_w) and total dynamical damping (DD_{total}) obtained for each reanalysis (year^{-1}), their ensemble mean and standard error, for 1980–2010

	DD_u	DD_v	DD_w	DD_{total}
CFSR	2.09 ± 0.12	−0.81 ± 0.00	−1.95 ± 0.05	−0.34 ± 0.08
ECDA	1.88 ± 0.10	−0.77 ± 0.00	−2.16 ± 0.05	−0.52 ± 0.08
GECCO2	1.73 ± 0.07	−0.69 ± 0.00	−1.06 ± 0.02	−0.01 ± 0.06
GODAS	3.22 ± 0.16	−0.85 ± 0.00	−2.56 ± 0.07	−0.09 ± 0.11
K7	1.97 ± 0.09	−0.77 ± 0.00	−2.59 ± 0.04	−0.69 ± 0.06
ORAS4	1.59 ± 0.13	−0.95 ± 0.00	−2.39 ± 0.05	−0.87 ± 0.09
SODA 3.4.1	−3.94 ± 0.16	−0.75 ± 0.00	−2.14 ± 0.09	−3.41 ± 0.13
ENS. MEAN	0.61 ± 0.44	−0.40 ± 0.02	−1.06 ± 0.10	−0.85 ± 0.44
Drifter/OSCAR	3.38 ± 0.41	−0.71 ± 0.31	No data	No data
SODA 2.0.2-4	−0.84 ± 0.39	−0.85 ± 0.07	−2.14 ± 0.20	−1.92 ± 0.22
NEMO-ORCA05	2.29 ± 0.22	−0.86 ± 0.05	−1.69 ± 0.15	−0.13 ± 0.14

The total dynamical damping is the sum of the individual terms divided by 2 (see Eq. 2). The values obtained by Lübbecke and McPhaden (2013) are shown in the lower section of the table

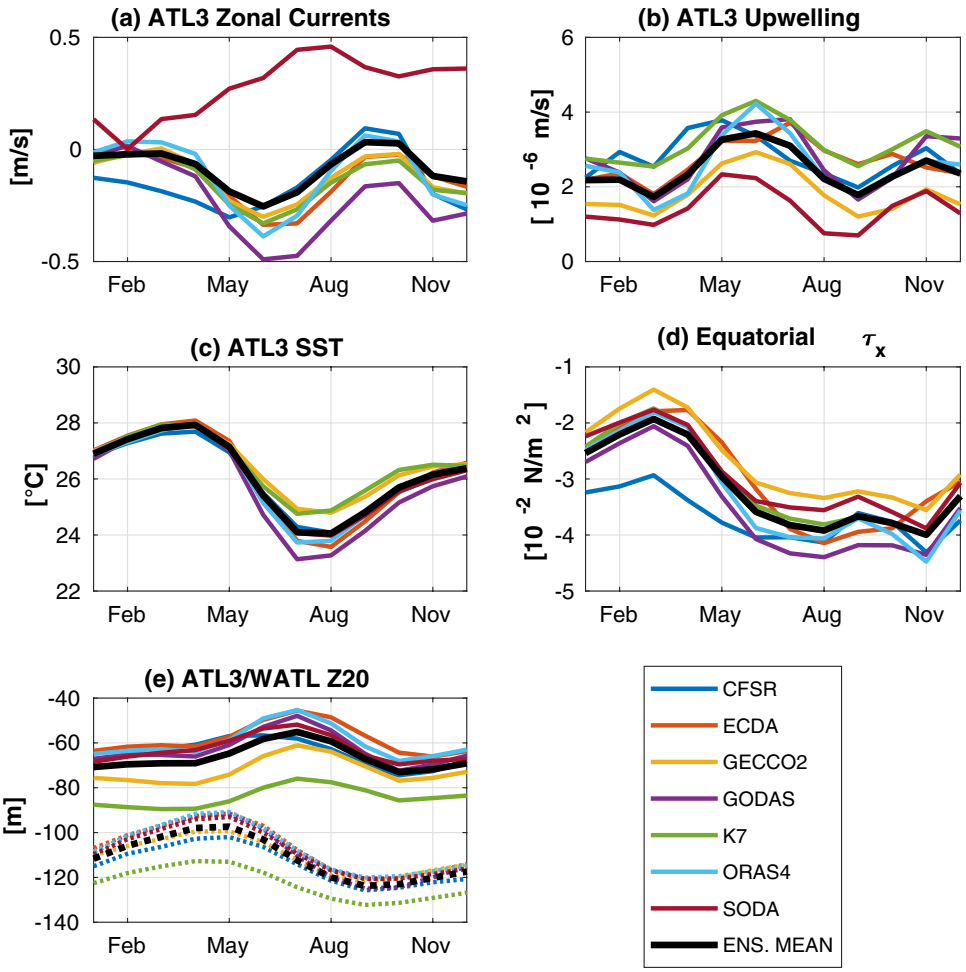

Fig. 3 Monthly climatologies (1980–2010) of the different parameters used in the calculation of the I_{BJ}: mean ATL3 surface zonal currents (**a**), mean ATL3 upwelling (**b**), mean ATL3 sea surface temperature (**c**), mean equatorial zonal wind stress (**d**), mean ATL3 (solid line) and WATL (dotted line) thermocline depth measured by the 20 °C isotherm depth (**e**) for each reanalyses and their ensemble mean

differences are observed among the zonal (DD_u), meridional (DD_v) and vertical (DD_w) components. SODA, however, is a clear outlier displaying an abnormally large positive zonal term. Figure 3a shows the monthly climatology of surface zonal currents in the ATL3 region for each reanalysis product. SODA displays large and eastward (positive) zonal currents throughout the year, as opposed to the other reanalyses, where the prevailing currents are westward. This occurs because its Equatorial Undercurrent extends all the way up to the surface, so that zonal velocities in the equatorial region as represented by this reanalysis are unrealistically large and eastward. The surface eastward currents in the SODA version used here (v3.4.1) are even larger than those in SODA v2.0.2 used by Lübbecke and McPhaden (2013), which explains the negative zonal DD term obtained here being larger than the one obtained in their study (-0.84 ± 0.39).

In all reanalyses the meridional term has the smallest contribution, while the vertical term dominates, resulting in a net damping effect. The only exception is SODA, for which the zonal damping term is even larger than the vertical term. As seen in Fig. 3b, of all the reanalyses, SODA is the one displaying the weakest upwelling in the ATL3 region year round. Despite this, its total DD term is the largest one, as a result of its large negative zonal term. The ensemble mean value obtained for the dynamical damping term ($-0.85 \pm 0.44\,\text{year}^{-1}$) falls between the values obtained by Lübbecke and McPhaden (2013) using NEMO-ORCA05 ($-0.13 \pm 0.14\,\text{year}^{-1}$) and SODA v2.0.2-4 ($-1.92 \pm 0.22\,\text{year}^{-1}$).

Thermal damping (TD) The coefficients calculated between the SST series from each reanalysis against NSHF data from TropFlux (Kumar et al. 2012) are shown in Table 3. The values converted to year^{-1} are summarized in Table 4. The correlation between NSHF and SST anomalies is negative, i.e., a positive SST anomaly in the ATL3 region leads to a negative NSHF anomaly, which acts to damp the SST anomaly, while a negative SST anomaly leads to a positive NSHF anomaly (Frankignoul and Kestenare 2002; Frankignoul et al. 2004). Correlations range from R = − 0.28 to R = − 0.52. The weakest correlation is observed for CFSR, which also has one of the smallest thermal damping terms. The largest thermal damping is obtained from ORAS4 ($-13.05 \pm 1.94\,\text{W m}^{-2}/^{\circ}\text{C}$ or $-1.44 \pm 0.21\,\text{year}^{-1}$),

Table 3 Regression parameters and the respective Pearson's correlation coefficient (brackets), for 1980–2010

	α [$Wm^{-2}/°C$]	μ_a [$10^{-2}\ Nm^{-2}/°C$]	β_u [ms^{-1}/Nm^{-2}]	β_w [$10^{-5}\ ms^{-1}/(Nm^{-2})$]	β_h [$10^2\ m/(Nm^{-2})$]	a_h [10^{-2} °C/m]
CFSR	−7.90 ± 2.42 (−0.28)	0.19 ± 0.07 (0.22)	4.91 ± 2.11 (0.21)	6.12 ± 1.41 (0.36)	8.23 ± 1.77 (0.39)	9.03 ± 0.32 (0.93)
ECDA	−11.44 ± 2.08 (−0.44)	0.44 ± 0.07 (0.48)	10.30 ± 1.28 (0.45)	6.20 ± 1.06 (0.47)	8.57 ± 0.87 (0.66)	10.99 ± 0.44 (0.91)
GECCO2	−12.16 ± 2.81 (−0.36)	0.44 ± 0.07 (0.50)	8.46 ± 1.17 (0.46)	5.15 ± 0.65 (0.58)	10.26 ± 0.87 (0.73)	6.89 ± 0.21 (0.95)
GODAS	−8.05 ± 1.93 (−0.35)	0.33 ± 0.06 (0.43)	19.70 ± 2.37 (0.42)	2.6 ± 0.67 (0.33)	10.12 ± 1.10 (0.64)	8.08 ± 0.34 (0.91)
K7	−10.89 ± 2.42 (−0.38)	0.54 ± 0.06 (0.60)	7.06 ± 1.23 (0.46)	7.55 ± 0.68 (0.71)	10.49 ± 0.73 (0.79)	7.93 ± 0.25 (0.94)
ORAS4	−13.05 ± 1.94 (−0.52)	0.59 ± 0.07 (0.61)	8.52 ± 0.65 (0.38)	4.98 ± 0.65 (0.57)	9.76 ± 0.67 (0.80)	11.01 ± 0.43 (0.92)
SODA 3.4.1	−10.07 ± 1.83 (−0.44)	0.35 ± 0.05 (0.51)	−1.67 ± 3.80 (0.08)*	4.63 ± 1.99 (0.21)	8.79 ± 1.50 (0.47)	7.25 ± 0.44 (0.83)
Observational data	−13.3 ± 6.7 (−0.47)	0.48 ± 0.22 (0.50)	2.99 ± 6.11 (0.18)	No data	No data	No data
SODA 2.0.2-4	−16.5 ± 6.8 (−0.56)	0.47 ± 0.19 (0.53)	18.76 ± 6.04 (0.63)	13.5 ± 9.4 (0.35)	8.5 ± 3.1 (0.58)	6.9 ± 0.01 (0.88)
NEMO-ORCA05	−12.4 ± 3.8 (−0.64)	0.86 ± 0.27 (0.63)	7.92 ± 1.55 (0.75)	2.8 ± 1.8 (0.33)	11.5 ± 1.9 (0.81)	3.8 ± 0.09 (0.78)

All correlations/regression coefficients are significant at the 95% level, with the exception of β_u for SODA (marked with an asterisk). The results obtained by Lübbecke and McPhaden (2013) are shown in the lower section of the table. Note that due to unavailable or scarce observational data for vertical velocities and thermocline depth, β_w could not be computed in their study, while β_h and a_h were not statistically significant

Table 4 I_{BJ} individual terms and total index for each reanalysis, their ensemble mean and standard error ($year^{-1}$), computed from Eq. 2, for 1980–2010

	DD	TD	ZAF	EF	TF	I_{BJ}
CFSR	−0.34 ± 0.08	−0.87 ± 0.27	0.03 ± 0.03	0.06 ± 0.01	0.15 ± 0.10	−0.96 ± 0.48
ECDA	−0.52 ± 0.08	−1.26 ± 0.23	0.27 ± 0.08	0.20 ± 0.00	0.46 ± 0.14	−0.85 ± 0.53
GECCO2	−0.01 ± 0.06	−1.34 ± 0.31	−0.04 ± 0.01	0.13 ± 0.00	0.21 ± 0.06	−1.04 ± 0.43
GODAS	−0.09 ± 0.11	−0.89 ± 0.21	0.37 ± 0.11	0.05 ± 0.00	0.44 ± 0.15	−0.12 ± 0.59
K7	−0.69 ± 0.06	−1.20 ± 0.27	0.36 ± 0.10	0.22 ± 0.01	0.62 ± 0.14	−0.69 ± 0.58
ORAS4	−0.87 ± 0.09	−1.44 ± 0.21	0.18 ± 0.04	0.20 ± 0.00	0.79 ± 0.18	−1.14 ± 0.52
SODA 3.4.1	−3.42 ± 0.13	−1.11 ± 0.20	−0.03 ± 0.05	0.10 ± 0.03	0.30 ± 0.11	−4.16 ± 0.53
ENS. MEAN	−0.85 ± 0.44	−1.16 ± 0.08	0.17 ± 0.07	0.14 ± 0.03	0.42 ± 0.08	−1.28 ± 0.50
SODA 2.0.2-4	−1.92 ± 0.22	−1.88 ± 0.08	0.04 ± 0.02	0.20 ± 0.16	0.38 ± 0.21	−3.19 ± 0.85
NEMO-ORCA05	−0.13 ± 0.14	−1.42 ± 0.43	0.09 ± 0.03	0.04 ± 0.03	0.51 ± 0.22	−0.91 ± 0.50

Results obtained by Lübbecke and McPhaden (2013) are shown in the lower section of the table

which also yields the largest correlation (R = − 0.52). This is consistent with the results obtained by Lübbecke and McPhaden (2013), who found a thermal damping in the ATL3 region ranging from −1.42 to −1.88 $year^{-1}$, using TropFlux combined with NOAA Optimum Interpolation SST (Reynolds SST), ERA-40 with SODA 2.0.2-4 and NEMO-ORCA05.

Zonal advective feedback (ZAF) The zonal advective feedback term depends on the parameters μ_a and β_u, which describe, respectively, the effect of SST anomalies on zonal wind anomalies and the effect of these wind anomalies on zonal current anomalies (Table 3).

Correlations are in general high for all products (0.48–0.61), except in CFSR, which displays the lowest correlation (R = 0.22) and the lowest value for μ_a ($0.19 \pm 0.07\ 10^{-2}\ Nm^{-2}/°C$). The strongest relationship is observed in ORAS4, with correlation R = 0.61 and $\mu_a = 0.58 \pm 0.07\ 10^{-2}\ Nm^{-2}/°C$. These values are similar to those found by Keenlyside and Latif (2007) ($0.75\ 10^{-2}\ Nm^{-2}/°C$) using HadISST and wind stress from NCEP-NCAR reanalysis and Lübbecke and McPhaden (2013) ($0.47–0.86\ 10^{-2}\ Nm^{-2}/°C$, using Reynolds SST with NCEP wind stress, SODA 2.0.2-4 and NEMO-ORCA05).

The parameter β_{uh} (response of zonal currents to thermocline adjustment) is not statistically significant in any of the products. For β_u (response to zonal wind stress), correlations vary greatly among the reanalyses. SODA (v.3.4.1) displays the weakest correlation (R = 0.08), as well as the lowest regression slope ($\beta_u = -1.67 \pm 1.83$ ms^{-1}/Nm^{-2}), which is not statistically significant, indicating this product does not capture well this relationship. This contrasts with the stronger relationship ($\beta_u = 18.76 \pm 6.04$ ms^{-1}/Nm^{-2}, R = −0.63) obtained by Lübbecke and McPhaden (2013) for SODA v.2.0.2-4. For all other reanalysis, the regressions are statistically significant at the 95% level. The second smallest correlation and regression slope are observed in CFSR (R = 0.21, $\beta_u = 4.91 \pm 2.11$ ms^{-1}/Nm^{-2}). All other products display relatively larger correlations (0.38-0.46) and regression coefficients (8.46–19.70 ms^{-1}/Nm^{-2}). These values are more similar to those obtained by Lübbecke and McPhaden (2013) using NEMO-ORCA05 (7.92 ± 1.55 ms^{-1}/Nm^{-2}).

Table 4 shows the total ZAF for each reanalysis. GECCO2 presents a positive mean zonal ATL3 SST gradient, as opposed to what is expected in this region. As a result, its ZAF term is negative (see Eq. 2). SODA also displays a negative ZAF, but this results from its negative β_u term. All other reanalysis show a positive ZAF, since this feedback acts to enhance the SST anomalies. The ensemble mean value found for ZAF (0.17 ± 0.07 year^{-1}) is larger than the values found by Lübbecke and McPhaden (2013) (0.02–0.09 *year*$^{-1}$), due to smaller zonal SST gradients in the ATL3 region found by the authors (−2.53 to -10.55×10^{-8} °Cm^{-1} against −5.93 to 0.54×10^{-7} °Cm^{-1} obtained here). As shown in Fig. 3c, there is a good agreement among the reanalyses in ATL3 SSTs in most of the year, except for JJA, when the spread is largest. This could contribute to the differences observed in the ZAF term.

Ekman feedback (EF) In addition to the effect of ATL3 SST anomalies on zonal equatorial wind anomalies (μ_a), the EF term also considers the influence of wind anomalies on upwelling in the ATL3 region (wind stress multiplied by − 1; Eq. 6). The regression parameters are shown in Table 3. Strong correlations are observed in GECCO2 (R = 0.58), K7 (R = 0.71) and ORAS4 (R = 0.57). SODA has the weakest correlation (R = 0.21) between zonal wind and upwelling anomalies. The value of β_w ranges from 2.6×10^{-5} to 7.55×10^{-5} ms^{-1}/(Nm^{-2}) among the reanalyses, similar to those obtained by Lübbecke and McPhaden (2013) ($2.80 \pm 1.80 \times 10^{-5}$ ms^{-1}/(Nm^{-2}) for SODA v2.0.2-4 and $13.5 \pm 9.4 \times 10^{-5}$ ms^{-1}/(Nm^{-2}) for NEMO-ORCA5).

The total EF term is shown in Table 4, for each reanalysis. EF is strongest in ECDA, K7 and ORAS4 (0.21, 0.22 and 0.20 year^{-1}, respectively), at least twice as as strong as in the remaining products. This feedback is weakest in CFSR (0.06 year^{-1}) and GODAS (0.05 year^{-1}) . The ensemble mean EF (0.14 ± 0.03 year^{-1}) falls between those those obtained by Lübbecke and McPhaden (2013) (0.20 and 0.04 year^{-1} for SODA 2.0.2 and NEMO-ORCA05, respectively). The EF is weaker than the ZAF in K7 and GODAS, but it is stronger than ZAF in GECCO2 and SODA, being similar to this term in the other reanalyses.

Thermocline feedback (TF). The thermocline feedback takes into account the effect of ATL3 SST on zonal equatorial winds (μ_a), their impact on zonal thermocline slope (β_h) and the impact of the resulting subsurface temperature anomalies on SSTs (a_h).

As shown in Table 3, CFSR and SODA have the weakest correlations between wind stress anomalies and thermocline slope (0.39 and 0.47, respectively). All other products display larger correlations, ranging from 0.66 (ECDA) to 0.80 (K7 and ORAS4, respectively). In spite of that, the regression coefficients found are similar among all products, ranging from 8.23×10^2 $m/(\mathrm{Nm}^{-2})$ (CFSR) to 10.49×10^2 $m/(\mathrm{Nm}^{-2})$ (K7). This could be related to differences in interannual variability among the reanalyses; since the correlation coefficient is the regression coefficient normalized by the data's standard deviation, if the correlations are different, different standard deviations could offset the differences in the correlation coefficient. As shown in Fig. 3d, there is also a considerable spread in monthly mean equatorial zonal wind stress among the reanalyses. The same is observed for the seasonal zonal thermocline slope: although the spread in seasonal WATL thermocline depth is not very large (Fig. 3e, dotted line), there is a considerable spread in ATL3 thermocline depth (Fig. 3e, solid lines).

For the response of ATL3 thermocline depth anomalies to subsurface temperatures (represented by a_h), correlations are very high in all products, ranging from 0.83 (SODA) to 0.95 (GECCO2). Regression slopes vary from 6.89×10^{-2} °C/m (GECCO2) to 11.01×10^{-2} °C/m (ORAS4).

The total TF for each reanalysis is shown in Table 4. In agreement to the results obtained by Lübbecke and McPhaden (2013) for SODA v2.0.2-4 and for NEMO-ORCA5, the TF is found to be the dominant positive feedback in all of the reanalyses. The ensemble mean TF is found to be 0.42 ± 0.08 while the ensemble mean EF is 0.14 ± 0.03, so that the difference between them is larger than their standard errors. The difference between them is also statistically significant at the 95% level.

Total Bjerknes Feedback Index (I_{BJ}). The individual components and the total I_{BJ} are summarized in Fig. 4 and in Table 4. The sum of all feedback terms yields a negative I_{BJ} in all reanalysis, with the exception of GODAS, for which it is zero. The negative I_{BJ} in all other reanalyses agrees with previous studies that show the Atlantic Equatorial Mode is damped (Zebiak 1993; Keenlyside and Latif 2007; Jansen

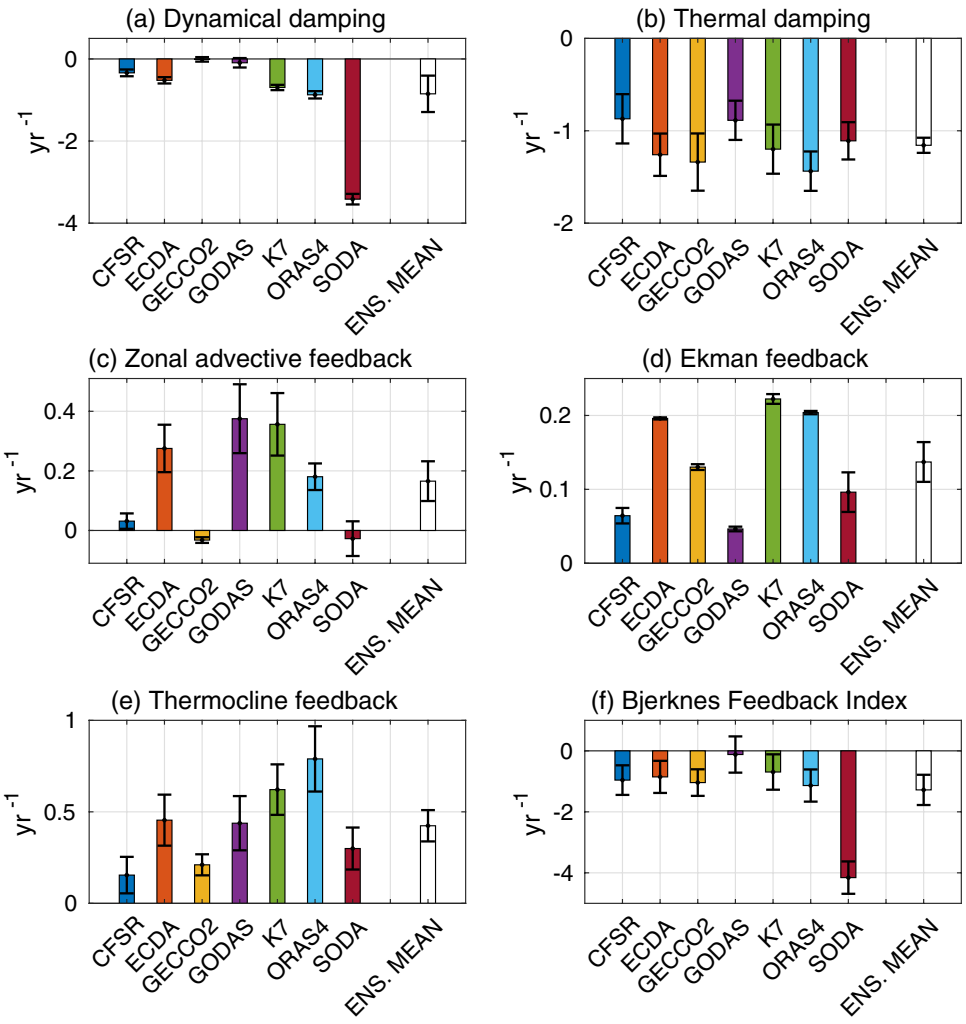

Fig. 4 Terms of the Bjerknes Feedback Index, computed for the whole time period (1980–2010): Dynamical damping (**a**), thermal damping (**b**), zonal advective feedback (**c**), Ekman feedback (**d**), thermocline feedback (**e**) and total Bjerknes Feedback Index (**f**), for each reanalysis and their ensemble mean. Error bars for the ensemble mean show the ensemble's standard error (ensemble standard deviation divided by the square root of the number of reanalyses)

et al. 2009; Lübbecke and McPhaden 2013). The greatest negative contribution comes from TD, in all reanalyses, except SODA, for which it comes from the unrealistic eastward equatorial zonal currents. The dominating TD in the other reanalysis products is consistent with the work of Nnamchi et al. (2015), who show that the a major part of the interannual variability of the equatorial mode is controlled by thermodynamical mechanisms ($68 \pm 23\%$ of the variance), while coupled dynamics plays a major role on its structure. It is worth noting however that other studies (Lübbecke et al. 2018, and references therein) have investigated the relative importance of dynamics and thermodynamics in driving Atlantic Niño events, concluding that despite a large variability being explained by thermodynamical processes, the dynamics and specifically the Bjerknes feedback are their main drivers.

The dominating positive feedback in all reanalyses is the thermocline feedback, which is consistent with the works of e.g. Keenlyside and Latif (2007), Lübbecke and McPhaden (2013) and Graham et al. (2014), who found the thermocline feedback is the strongest positive feedback in the Tropical Atlantic. Despite this, the contribution of all positive terms (i.e., those which enhance variability) is consistently weaker than the damping mechanisms. The most damped total feedback was found for SODA ($-4.16 \pm 0.53\,\text{year}^{-1}$), although this is most likely not realistic, as discussed above. After SODA, the most damped I_{BJ} is found for ORAS4 ($-1.14 \pm 0.52\,\text{year}^{-1}$). The least damped is the one obtained from GODAS, which is statistically zero ($-0.12 \pm 0.59\,\text{year}^{-1}$), due to its weaker combination of its damping terms. The ensemble mean I_{BJ} obtained is $-1.28 \pm 0.50\,\text{year}^{-1}$, which falls between the values obtained by Lübbecke and McPhaden (2013) for SODA 2.0.2-4 ($-3.19 \pm 0.85\,\text{year}^{-1}$) and NEMO-ORCA05 ($-0.91 \pm 0.50\,\text{year}^{-1}$).

4.2 Differences between 1980–1999 and 2000–2010

In this section we investigate the weakening in the tropical Atlantic variability observed over the last decades reported by Tokinaga and Xie (2011) and Prigent et al. (2020) in terms of the I_{BJ}. A shift in ENSO towards more frequent and weaker Modoki events has been reported after 2000 (e.g., Hu et al. 2013), which was assessed by Lübbecke and McPhaden (2014) in terms of changes in the I_{BJ} between 1980–1999 (P1) and 2000–2010 (P2). In this section, we look for similar changes in terms of the I_{BJ} in the same periods for the Tropical Atlantic, in light of the weakening in the Atlantic cold tongue reported by Tokinaga and Xie (2011) and weakened SST variability in this region after 2000 (Prigent et al. 2020).

Indeed, as shown in Fig. 5a, b, the ensemble mean spatial pattern of the equatorial mode is much weaker in 2000-2010 compared to 1980–1999, which indicates a weakening in the equatorial mode for this period. The region where there is more agreement among the reanalyses in the statistical significance of the correlation (stippled region in Fig. 5b) also shrinks in the recent period, indicating this weakening is consistent. This is further reinforced by Fig. 5c, d, which depict the ensemble mean standard deviation of JJA SST anomalies in P1 and its percentual reduction in P2, revealing a decrease in variability of around 30% in the eastern equatorial region, similar to the results obtained by Prigent

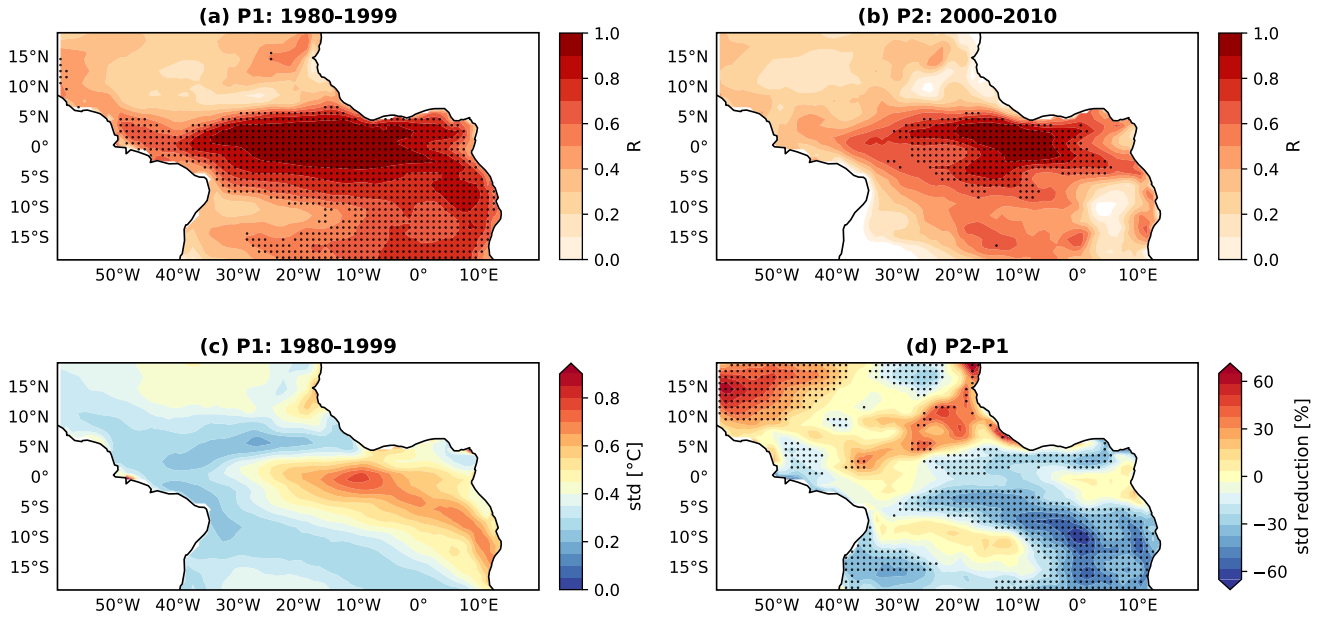

Fig. 5 Spatial pattern of the Atlantic equatorial mode averaged in JJA for **a** 1980–1999 and **b** 2000–2010, for the ensemble mean. The pattern is obtained by correlating the ATL3 index series (mean SST anomaly in the ATL3 region) against SST anomalies elsewhere. Stippling indicates regions where the correlations are significant in at least 5 of the 7 reanalyses, at the 95% level. JJA standard deviation of SSTs in P1 (**c**) and the percentual reduction in P2 compared to P1 (**d**). Stippling in **d** indicates regions where the difference between the two periods is significant at the 95% level of a Welch's t-test

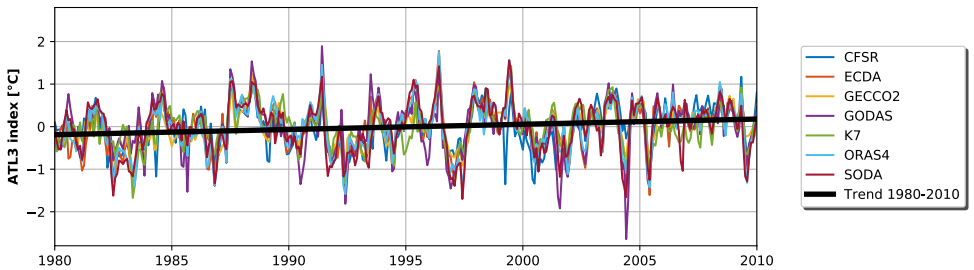

Fig. 6 Time series of the ATL3 index (SST anomalies average over the ATL3 region) for each reanalysis. In each period, only one of the reanalyses do not show significant trends (GODAS in P1 and K7 in P2). The ensemble mean trends for the 1980–1999 period (black, $0.017 \pm 0.005°C/mon^{-1}$) and 2000–2010 period (red, $0.052 \pm 0.011°C/mon^{-1}$) are also shown; the difference between them is significant at the 95% level

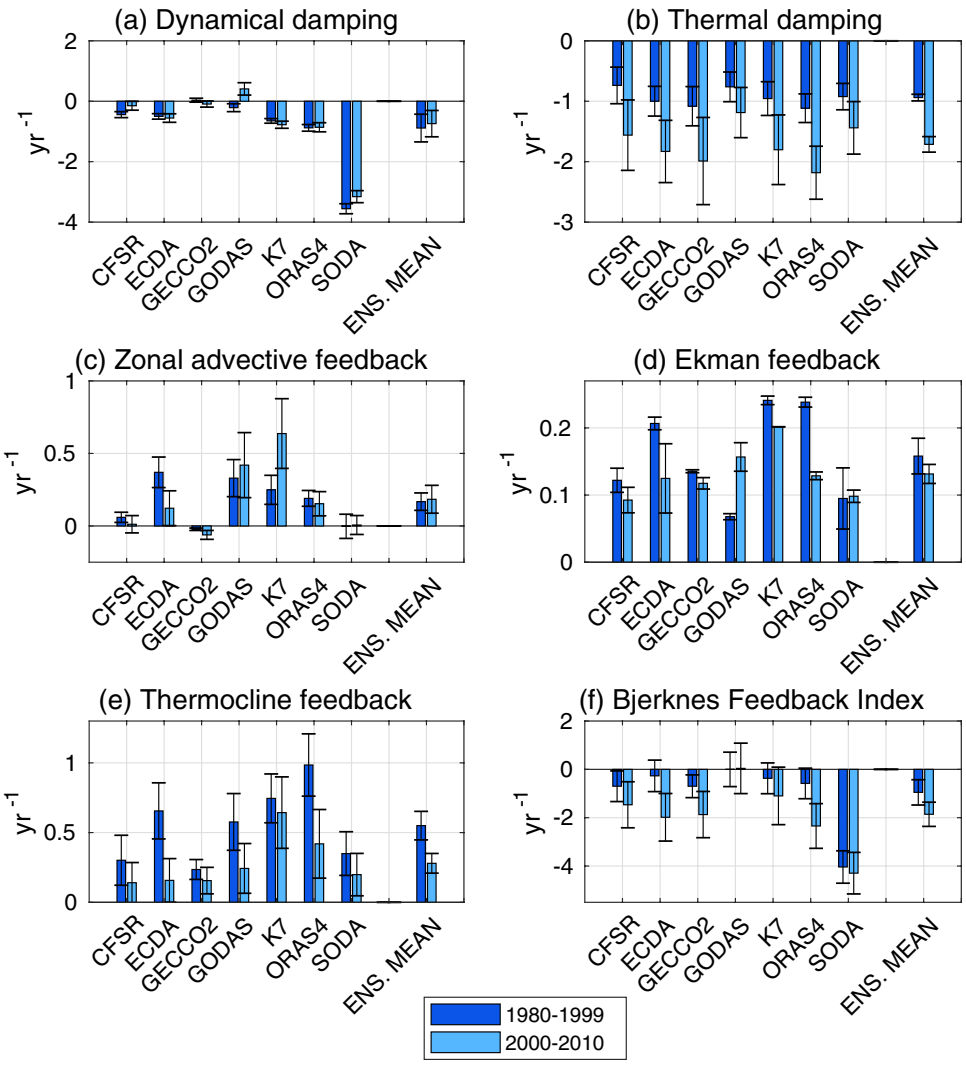

Fig. 7 Dynamical damping (**a**), thermal damping (**b**), zonal advective feedback (**c**), Ekman feedback (**d**), thermocline feedback (**e**) and total Bjerknes Feedback Index (**f**), for 1980–1999 (dark blue) and 2000–2010 (light blue) for each reanalysis and their ensemble mean. The ensemble error bar represents the ensemble standard error

et al. (2020). In addition, a warming trend is observed throughout the period analyzed (Fig. 6, ensemble mean is $0.0123 \pm 0.002\,°\text{Cmon}^{-1}$). The ensemble mean ATL3 SST anomaly in P2 is also positive, while in P1 it is negative ($0.07 \pm 0.02\,°\text{C}$ in P2 against $-0.04 \pm 0.01\,°\text{C}$ in P1). This difference is significant at the 95% level according to a two-tailed t-test.

The comparison between I_{BJ} and each of its components in 1980–1999 and 2000–2010 is shown in Fig. 7. Regarding the negative (damping) terms, there are no visible changes in DD (Fig. 7a) in comparison to the earlier period, with some products showing a stronger and others a weaker DD term in 2000–2010. The error bars are overlapping in the ensemble mean total DD and for all three components (zonal, meridional and vertical) the ensemble error of each period is larger than the difference between the time periods (not shown). On the other hand, a stronger TD is observed in all reanalyses in the more recent period (Fig. 7b), compared to the earlier period. The ensemble mean shows a much stronger thermal damping in 2000–2010 ($-1.58 \pm 0.14\,\text{year}^{-1}$) compared to 1980–1999 ($-0.96 \pm 0.07\,\text{year}^{-1}$). The error bars do not overlap and the difference between the time periods ($-0.61\,\text{year}^{-1}$) is larger than the ensemble standard errors (0.07 and $0.14\,\text{year}^{-1}$). The difference between P1 and P2 is also significant at the 95% level of a two-tailed t-test.

For the positive terms, the ensemble mean ZAF (Fig. 7c) is the same for both periods. There is some disagreement among the reanalyses regarding EF, as CFSR, GECCO2 and SODA remain unchanged, ECDA, K7 and ORAS4 display a weakening while GODAS display a strengthening (Fig. 7d). As a result, no changes are observed in this term in the ensemble mean, with the difference between the two time periods ($0.02\,\text{year}^{-1}$) being the same as the standard error in P1. For TF (Fig. 7e), all reanalysis products present a weakening in the last period, although most of them within the error bars; however, considering the ensemble mean, there is a consistent weakening in P2 (a decrease of $0.3\,\text{year}^{-1}$ while the ensemble standard errors are $0.1\,\text{year}^{-1}$ for both periods).

The difference between the samples for each period is also significant at the 95% level of a two-tailed t-test.

As a result, the total I_{BJ} (Fig. 7f) is more negative (i.e., the system is more damped) in 2000-2010 for all reanalyses, except GODAS, for which the total index is zero in both periods, and SODA, for which the total I_{BJ} is very similar in both periods. The ensemble mean I_{BJ} was found to be $-0.95 \pm 0.52\,\text{year}^{-1}$ in 1980–1999 and $-1.86 \pm 0.50\,\text{year}^{-1}$ in 2000–2010. Interestingly, despite the consistent strengthening of the thermal damping term and weakening of the thermocline feedback, this difference is not significant (95% level of a two-tailed t-test) and the ensemble's standard error intervals from each period overlap; This is due to the unrealistic large DD obtained from SODA. If all reanalyses but SODA are considered, the ensemble means for P1 and P2 are $-0.44 \pm 0.11\,\text{year}^{-1}$ and $-1.45 \pm 0.35\,\text{year}^{-1}$; in this case, the error bars do not overlap and the difference in the total I_{BJ} between P1 and P2 is statistically significant at the 95% level. This reinforces the hypothesis that the system is more damped in the recent period.

The results considering a longer second period for ORAS4 (2000–2017) and GODAS (2000–2018) lead to the same conclusion. The I_{BJ} weakens in the recent period in both reanalyses, yielding $-2.07 \pm 0.69\,\text{year}^{-1}$ in 2000–2017 against $-0.60 \pm 0.63\,\text{year}^{-1}$ in 1980–1999 in ORAS4 and $-0.16 \pm 0.76\,\text{year}^{-1}$ in 1980–1999 against -0.69 ± 0.95 $year^{-1}$ in 2000–2018 in GODAS. Both reanalyses also show a stronger TD and weaker TF considering a longer second period. The thermal damping term increases from $-1.09 \pm 0.24\,\text{year}^{-1}$ to $-1.88 \pm 0.81\,\text{year}^{-1}$ in ORAS4 and from $-0.69 \pm 0.25\,\text{year}^{-1}$ to $-1.14 \pm 0.30\,\text{year}^{-1}$ in GODAS, while the TF term decreases from $0.94 \pm 0.22\,\text{year}^{-1}$ to $0.35 \pm 0.18\,\text{year}^{-1}$ in ORAS4 and from $0.62 \pm 0.22\,\text{year}^{-1}$ to $0.30 \pm 0.18\,\text{year}^{-1}$ in GODAS. Although these changes are within the error intervals, they follow the same pattern observed for the same reanalyses comparing 1980–1999 to 2000–2010.

In order to understand the changes in the feedback terms, we turn to the respective regression coefficients. The parameters α, μ_a, β_h and a_h, which are associated with TD and TF, are shown in Fig. 8, for each time period.

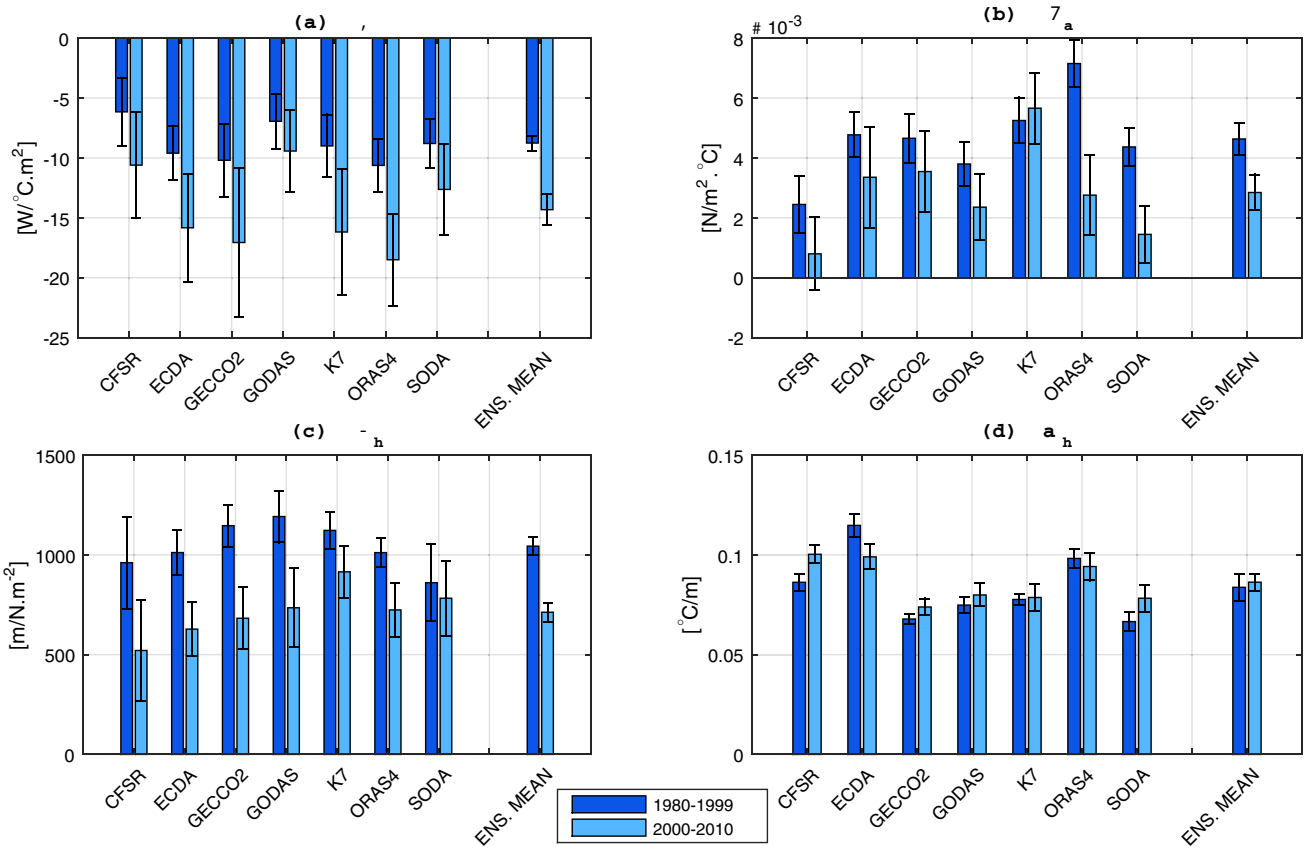

Fig. 8 Regression parameters associated with TD and TF for 1980–1999 (dark blue) and 2000–2010 (light blue) for each reanalysis and their ensemble mean: thermal damping (**a**), equatorial zonal wind stress response to ATL3 SST anomalies (**b**), equatorial thermocline slope response to zonal wind stress anomalies (**c**) and SST response to subsurface temperature anomalies (**d**). The error bars indicate the regression standard error for each reanalysis and the ensemble standard error for the ensemble mean

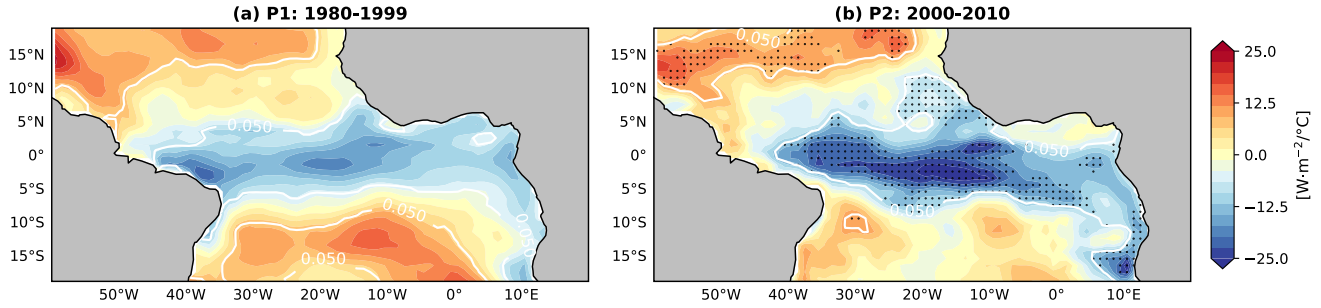

Fig. 9 Pointwise linear regression of the reanalyses ensemble mean SST anomalies against TropFlux NSHF anomalies, for **a** 1980–1999 and **b** 2000–2010. White contours denote the regions where regressions are significant at the 95% level and stippling in **b** indicates regions where the difference between P1 and P2 is significant at the 95% level

The stronger thermal damping in 2000–2010 observed in Figs. 8a and 7b is corroborated by the analysis of the spatial regression patterns between TropFlux NSHF anomalies and the reanalyses ensemble mean SST anomalies for the two time periods (Fig. 9). Consistent with the stronger thermal damping, there is a strengthening in the regression pattern, with significant increase in absolute values (95% level) ranging from -5 to $-15\,\mathrm{W}\cdot m^{-2}/°\mathrm{C}$ in the equatorial region in P2. This could be a result of the long term warming of the region (Fig. 6), leading to increased evaporative damping through increased latent heat flux (Tokinaga and Xie 2011; Servain et al. 2014). A detailed analysis of heat flux changes by Prigent et al. (2020) shows as well that the stronger net heat flux damping is due to the increased latent heat flux; they also find that the although the TD is influenced by both the latent heat flux damping and winds, the stronger TD after 2000 is mainly due to a stronger response of latent heat fluxes to SST anomalies, which in turn is due to an increased response of near-surface specific humidity difference.

Although no changes are observed in a_h (Fig. 8d), the other two parameters that constitute the TF display a difference larger than the ensemble standard error between the two periods analyzed. The term μ_a shows a decrease in the recent period for all products except K7 (Fig. 8b). This weakening is robust in ORAS4 and SODA (non-overlapping error

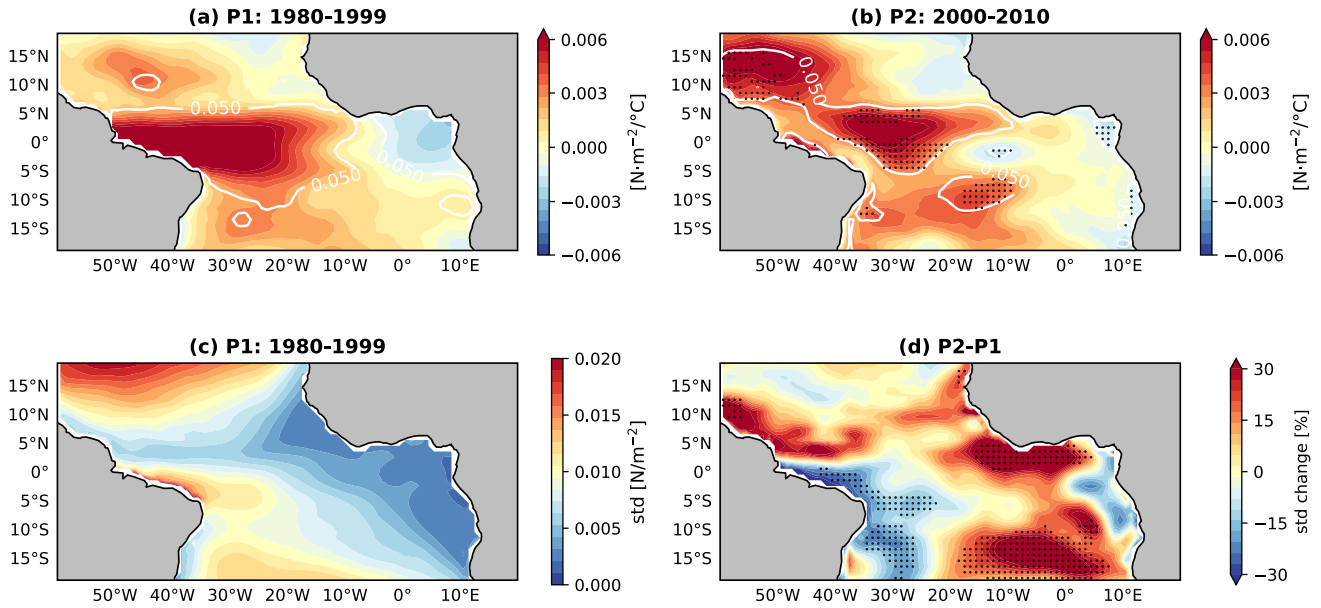

Fig. 10 Regression of ATL3 SST anomalies and zonal wind stress elsewhere in the basin, for **a** 1980–1999 and **b** 2000–2010. White contours denote the regions where regressions are significant at the 95% level and stippling in **b** indicates regions where the difference between P1 and P2 is significant at the 90% level; MAM standard deviation of zonal wind stress in P1 (**c**) and the percentual reduction in P2 compared to P1 (**d**). Stippling in **d** indicates regions where the difference between the two periods is significant at the 95% level of a Welch's t-test

bars), as well as in the ensemble mean ($0.46 \pm 0.05 \times 10^{-2}$ $N \cdot m^{-2}/°C$ in 1980–1999 against $0.28 \pm 0.06 \times 10^{-2}$ $Nm^{-2}/°C$ in 2000–2010).

The regression between ATL3 SST anomalies and zonal wind stress anomalies elsewhere in the basin in the two periods is shown in Fig. 10a, b. Positive regressions/correlations (red regions) indicate that a positive ATL3 SST anomaly induces a positive (eastward) zonal wind stress anomaly, that is, a weakening in the zonal winds. Likewise, negative ATL3 SST anomalies drive a negative (westward) zonal wind anomaly, i.e., stronger zonal winds. The opposite happen for negative correlations. A consistent weakening and eastward displacement of western zonal wind stress response to eastern SST anomalies is observed in the recent period. This explains the smaller μ_a in 2000–2010, as it is the regression of equatorially averaged zonal wind stress anomalies against ATL3 SST anomalies. A weaker variability in zonal wind stress in the western equatorial region is also observed in P2 compared to P1 (Fig. 10c, d), which is most likely related to the weaker SST variability. Although there is an increase in the standard deviation in P2 along the southern coast of Western Africa and in the southern Tropical Atlantic, it is not clear if these changes are related to the decreased SST variability in the ATL3 region. The weaker western zonal wind-SST relationship may be a result of the warming of the tropical north Atlantic, which shifts the rainfall band associated with the ITCZ and the wind-evaporation SST feedback (Maeda et al. 2016; Amaya et al. 2017). A northward shift in the ITCZ is also suggested by Prigent et al. (2020) as one of the reasons for the weaker zonal wind–SST relationship after 2000.

As a side note, the region of negative correlations off the coast of Africa also diminishes in the recent period (Fig. 10b). This region is associated with the impact of the EEA SSTs on the West Africa Monsoon via an intensification/weakening of the land–ocean atmospheric pressure gradient as a result of negative/positive SST anomalies (Xie and Carton 2013). Therefore, the weaker correlation in this region could indicate a weaker influence of the SST anomalies on the monsoon, although more detailed work would be necessary to confirm this.

For β_h, a decrease in 2000–2010 is observed in all reanalyses, with non-overlapping error bars in ECDA, GECCO2, GODAS and ORAS4, the same happening with the ensemble mean ($10.43 \pm 0.44 \times 10^2\, m/(Nm^{-2})$ in 1980–1999 against $7.12 \pm 0.47 \times 10^2\, m/(Nm^{-2})$ in 2000–2010). The regression between mean equatorial wind stress anomalies and thermocline anomalies are shown in Fig. 11. Positive regressions/correlations indicate that a positive zonal wind stress anomaly (eastward) lead to positive thermocline depth anomalies, i.e., a deepening of the thermocline (and negative wind stress anomalies, i.e., stronger winds lead to a shoaling of the thermocline). The opposite happens in the regions of negative correlations. The regression between mean equatorial wind stress anomalies and thermocline depth anomalies (Fig. 11) shows a weaker pattern in 2000–2010, with the region of positive correlations more concentrated at the equator and displaying lower values for the regression coefficient. There is also a weakening in P2 in the negative regression in the western equatorial region, which is statistically significant at the 90% across the reanalysis products. Therefore, the weaker thermocline feedback in the recent period could be associated with a weaker response of the thermocline slope to anomalous zonal wind stress in the equatorial region.

One possible explanation for the change in the wind-thermocline relation is the sensitivity of thermocline changes to the forcing of different baroclinic modes related to the vertical stratification. As discussed in Illig et al. (2004); Illig and Bachèlery (2019); Illig et al. (2020), interannual variability in the EEA is dominated by the second baroclinic mode associated with the planetary waves triggered by anomalous wind stress in the central-western side of the basin. Therefore, the change in the wind-thermocline relation could be related to differences in the structure of the wind forcing and

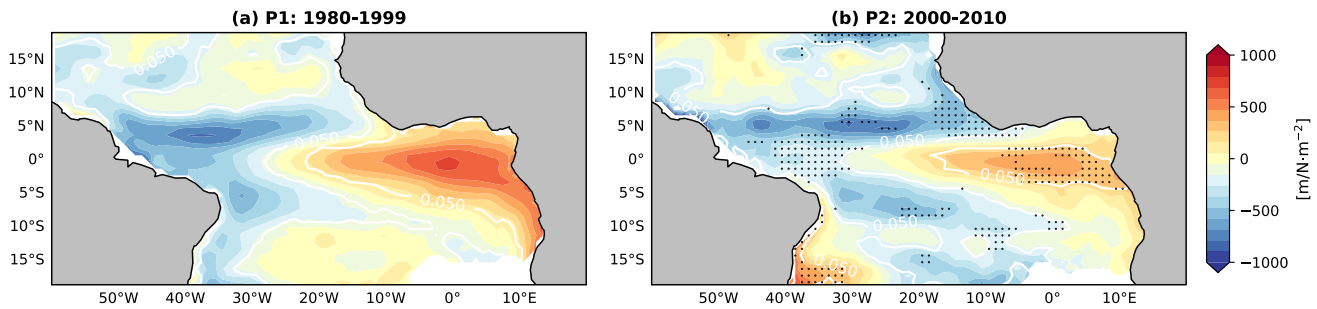

Fig. 11 Regression of mean equatorial zonal wind stress and thermocline depth (Z20), for **a** 1980–1999 and **b** 2000–2010. White contours denote the regions where regressions are significant at the 95% level and stippling in **b** indicates regions where the difference between P1 and P2 is significant at the 90% level

vertical structure of the ocean. More detailed analyses would be needed in future works.

The results for the different feedback terms show that the more damped I_{BJ} in 2000–2010 is related to a weaker thermocline feedback and a stronger thermal damping. This is consistent with results obtained by Tokinaga and Xie (2011), which associate the decrease in the ACT variability with a weaker thermocline feedback, due to a decreased zonal thermocline slope resulting from weaker trade winds, and increased upward net heat flux, leading to a stronger evaporative damping of SSTs. This also agrees with results obtained by Servain et al. (2014), who argue that long term SST warming in this region drives an increase in the surface latent heat flux. However, while the former associated the warming of the ACT with weaker trades, the latter argues that increases in SST enhance convection, accelerating the hydrological cycle and strengthening the trade winds. In the reanalyses considered here, no consistent trends are found for the equatorial zonal wind stress: out of the 7 reanalyses, only four showed significant trends according to a Mann–Kendall test (i.e., CFSR, GECCO2, ORAS4 and SODA), the trends observed in the first three being positive and the trend observed in SODA being negative (Fig. 12).

A weakening in the Bjerknes Feedback in the Pacific in the same time periods as considered here are reported by Lübbecke and McPhaden (2014). However, the weaker Bjerknes Feedback in the Pacific was found to be a result of a weaker thermocline feedback only, without any changes in thermal damping, which further reinforces the important role of thermodynamics in shaping variability in the equatorial Atlantic (Nnamchi et al. 2015, 2016). The weaker total feedback was associated with a weaker thermocline feedback, but unlike the results obtained here for the Atlantic, this was shown to be a result of a cooler eastern Pacific, leading to a westward shift of the ascending branch of the Pacific Walker cell and a westward confinement of the wind stress response to eastern Pacific SST anomalies.

The weaker thermocline feedback discussed here for the Atlantic could be associated with the positive phase of the AMO in the more recent period: according to Martín-Rey et al. (2018), the positive phase of the AMO leads to a deeper thermocline in the eastern an central equatorial Atlantic, while the negative phase leads to a shallower thermocline. However, in the reanalysis products considered here, we do not observe any significant change in the ATL3 thermocline depth; instead, there is a consistent shoaling trend in the WATL thermocline depth (not shown) and its anomalies are statistically different in P2 in comparison with P1, but the same is not observed for the ATL3 thermocline, neither for ATL3 upwelling. Despite this, the response of the thermocline to equatorial zonal wind stress appears to weaken in the recent period both in the WATL and the ATL3 regions, as shown in Fig. 11. So, despite an apparent weakening, the reason why it occurs in the ATL3 region is not clear from our data. No changes in the mean thermocline depth or mean zonal wind stress in P2 are found either.

It is important to note that the periods considered here are rather short, in particular P2. The several variables required to compute the I_{BJ} are not always available for long periods, or for the same periods in different reanalysis products; using an ensemble of different reanalysis datasets is preferred, since the individual errors are quite large. The short periods taken into account in the ensemble analysis raise the question of whether the observed changes in the I_{BJ} are due to sampling of stochastic atmospheric variability. Despite the results discussed above for a ORAS4 and GODAS considering a longer time period suggesting otherwise, as more reanalysis products spanning longer time periods become available, an ensemble analysis over two periods of at least 20 years each should be carried.

Another limitation is the fact that the I_{BJ} is a linear approximation of the dynamics underlying ENSO-like variability. As discussed by Graham et al. (2014), the I_{BJ} misrepresents the true magnitude of the individual feedback terms, overestimating the contribution of the thermocline feedback over the zonal advective feedback. Instead, they suggest the direct analysis of the mixed layer heat budget feedbacks on which the I_{BJ} is based may be more reliable.

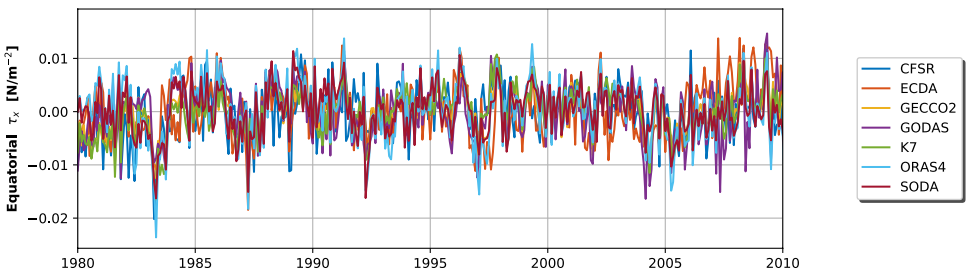

Fig. 12 Time series of zonal wind stress anomalies averaged in the equatorial region (3°N–3°S; 40°W–0°) for each reanalysis. CFSR, GECCO2 and ORAS4 only show significant positive trends at the 95% (i.e., weakening of the trade winds), while SODA shows a negative trend and the remaining reanalyses do not show any significant trend for 1980–2010

Furthermore, as shown by Richter et al. (2013), some Atlantic Niño events are not explained by the Bjerknes Feedback, but rather appear to be related to meridional advection of temperature anomalies from the northern Tropical Atlantic. Other mechanisms behind such events include off-equatorial Rossby waves reflected at the western boundary as equatorial Kelvin waves, net surface heat flux forcing and influences of the equatorial deep jets,as summarized by Lübbecke et al. (2018, and references therein). Therefore changes in the Bjerknes Feedback alone may not be sufficient to infer changes in variability in the Tropical Atlantic.

Despite this, previous studies (e.g., Tokinaga and Xie 2011; Martín-Rey et al. 2018; Prigent et al. 2020) have found a weaker Bjerknes feedback to be associated with weaker variability in this region, while Lübbecke and McPhaden (2014) found a weaker I_{BJ} associate with weaker variability in ENSO after 2000. In addition, the fact that most of the reanalyses used (5 out of 7) agree in the weaker total I_{BJ} and all of them show a weaker thermocline feedback and stronger thermal damping in P2, in agreement with the results obtained by Prigent et al. (2020) for 2000–2017, indicates some robustness in our results, although ideally the analysis should be performed over a longer time period. Further work should also consider an analysis of mixed-layer heat budget changes.

5 Summary and conclusions

In this study we assessed the Bjerknes Feedback in terms of its Index in the Tropical Atlantic as represented in a group of seven reanalyses from the Ocean Reanalysis Intercomparison Project (ORA-IP—Balmaseda et al. 2013), for the period 1980–2010. The same index is used to quantify changes in this feedback between 1980–1999 (P1) and 2000–2010 (P2).

While there are significant differences among the individual reanalysis products, their ensemble mean show the Atlantic equatorial mode is damped (negative total I_{BJ}), which is consistent with previous works (e.g., Zebiak 1993; Keenlyside and Latif 2007; Jansen et al. 2009; Lübbecke and McPhaden 2013). The mechanisms that act to damp the Atlantic equatorial mode are the effect of mean climatological currents (dynamical damping) and the air-sea heat flux exchange (thermal damping). The thermal damping is the dominating damping mechanism in all of the reanalyses, with the exception of SODA (v3.4.1), which shows a stronger dynamical damping. This is due to the fact that it represents the equatorial undercurrent extending all the way up to the surface; the unrealistic damping caused by these mean eastward currents ($-3.94 \pm 0.16\,\text{year}^{-1}$), instead of the expected westward mean zonal currents which would otherwise offset to some extent the damping by upwelling and meridional currents, leads to an abnormally large total dynamical damping term. This is even larger than the negative zonal term obtained by Lübbecke and McPhaden (2013) using SODA v2.0.2-4 ($-0.84 \pm 0.39\,\text{year}^{-1}$). Consequently, we conclude this reanalysis product should be used with caution in studies of the tropical Atlantic. The remaining reanalysis products are in agreement with previous studies (e.g., Lübbecke and McPhaden 2013; Nnamchi et al. 2015), in that they show a larger contribution of the thermal damping term, compared to the dynamical one.

Regarding the positive feedback terms, there is no agreement among the reanalysis regarding the relative importances of the zonal advective (ZAF) and Ekman feedback (EF) terms. In addition, errors in the representation of the mean zonal SST gradients in the eastern equatorial Atlantic region, which is known to shown large biases (Richter and Xie 2008; Richter et al. 2012, 2014), may lead to unrealistic values of the ZAF: due to a positive SST gradient in the ATL3 region used to compute the ZAF, this term is negative in GECCO2 as opposed to the expected positive value. This term is negative in SODA v3.4.1 too; however, in this case it is related to a negative zonal wind-zonal current anomalies relationship (β_u); the regression between the two variables is not significant in SODA v3.4.1, so the ZAF obtained from this reanalysis is not reliable either. On the other hand, more consistency is observed for the thermocline feedback among the different reanalysis products: it is the dominating positive feedback in all of them, in accordance with the works of Keenlyside and Latif (2007); Lübbecke and McPhaden (2013); Graham et al. (2014).

We then investigate the changes in the equatorial mode of the Atlantic in the recent decades using the reanalyses ensemble. A weakening of the ACT in the last six decades was reported by Tokinaga and Xie (2011), associated with weaker interannual variability and a weaker thermocline feedback driven by weaker trade winds and higher SSTs in the EEA. Weakened SST variability associated with a weaker Bjerknes Feedback after 2000 in the Tropical Atlantic is also discussed by Prigent et al. (2020). In our results, the ensemble mean ATL3 SST anomaly for 2000-2010 (P2) is positive, while the ensemble mean for P1 (1980-1999) is negative. In addition, the spatial pattern of the Atlantic equatorial mode showed a robust weakening in P2 compared to P1, as well as the standard deviations of boreal winter ATL3 SST anomalies (30% reduction). Indeed, the computation of the I_{BJ} yielded a more negative index for the recent period ($-1.86 \pm 0.50\,\text{year}^{-1}$ in 2000–2010 against $-0.95 \pm 0.52\,\text{year}^{-1}$ in 1980–1999, for the ensemble mean), as a result of the stronger thermal damping ($-1.71 \pm 0.13\,\text{year}^{-1}$ in 2000–2010 against $-0.94 \pm 0.06\,\text{year}^{-1}$ in 1980–1999) and a weaker thermocline feedback ($0.28 \pm 0.07\,\text{year}^{-1}$ in 2000–2010 against $0.55 \pm 0.10\,\text{year}^{-1}$ in 1980–1999). The stronger thermal damping in P2 appears to be a response to the warming of

the ACT, as suggested by Servain et al. (2014). The analysis of the individual net surface heat flux components by Prigent et al. (2020) shows that the main contribution comes from the increased latent heat flux.

The weaker thermocline feedback, on the other hand, is found to be related to a weaker response of western zonal wind stress anomalies to ATL3 SST anomalies. This response is displaced eastward in P2. Variability of zonal wind stress in the western equatorial region has also decreased, which is probably related to the decreased variability in ATL3 SSTs. The weaker wind-SST response in P2 could be related to a warmer northern Tropical Atlantic and a northward shift in the ITCZ (Maeda et al. 2016; Amaya et al. 2017; Prigent et al. 2020). A weaker response of the equatorial thermocline to anomalous equatorial zonal wind stress was also observed in P2. However, no consistent trends are found for the EEA thermocline depth (ATL3 region) in the period analyzed, but rather, a shoaling trend in the western equatorial (WATL region) is observed in all reanalyses. The reason why there is a decrease in the ATL3 thermocline response to anomalous wind stress is not clear, since no changes in ATL3 thermocline anomalies of its mean state are found for P2 in our data. No mean state changes were observed for zonal wind stress either. The weaker thermocline-wind relation could be associated to changes in the forcing of the thermocline by different baroclinic modes, which should be investigated further.

It is important to note that the short time period considered here was the common period covered by all the reanalyses and that a longer period would be desired. Nonetheless, the ensemble analysis showed results consistent with previous studies (e.g., Tokinaga and Xie 2011; Prigent et al. 2020) (i.e., weaker thermocline feedback and stronger thermal damping). Finally, it is worth noting that the I_{BJ} is a linear simplification of the dynamics underlying the Atlantic equatorial mode, based on the mixed layer heat budget, and has been suggested to misrepresent the relative importances of the individual feedback terms (Graham et al. 2014). Moreover, other processes at play in Tropical Atlantic variability (Richter et al. 2013; Lübbecke et al. 2018) could make the I_{BJ} analysis insufficient to assess changes in variability. Therefore, further work should considered a mixed layer heat budget analysis of the weaker variability after 2000, as well as the role of mechanisms other than the Bjerknes Feedback that are relevant for the Tropical Atlantic variability.

Acknowledgements This study was supported by Coordenação de Aperfeiçoamento de Pessoal de Nível Superior - Brasil (CAPES) grant 001. Ilana Wainer was supported by grants FAPESP (Fundação de Amparo à Pesquisa do Estado de S. Paulo) 215/17659-0 and 18/14789-9 CNPq:301726/2013-2, 405869/2013-4 and CNPq (Conselho Nacional de Desenvolvimento Científico e Tecnológico)-MCT-INCT-594 CRIOSFERA 573720/2008-8.

Author Contributions IW and PS designed the study. PS performed the analysis and wrote the manuscript draft. All authors contributed to the interpretation of the results and to the improvement of the manuscript.

Compliance with ethical standards

Conflict of interest The authors declare that they have no conflict of interest.

References

Amaya DJ, DeFlorio MJ, Miller AJ, Xie SP (2017) WES Feedback and the Atlantic Meridional Mode: observations and CMIP5 comparisons. Clim Dyn 49(5):1665–1679. https://doi.org/10.1007/s00382-016-3411-1

Back LE, Bretherton CS (2009a) a simple model of climatological rainfall and vertical motion patterns over the tropical oceans. J Clim 22(23):6477–6497. https://doi.org/10.1175/2009JCLI2393.1, https://journals.ametsoc.org/jcli/article-pdf/22/23/6477/3953158/2009jcli2393_1.pdf

Back LE, Bretherton CS (2009b) On the relationship between SST gradients, boundary layer winds, and convergence over the tropical oceans. J Clim 22(15):4182–4196, https://doi.org/10.1175/2009JCLI2392.1. https://journals.ametsoc.org/jcli/article-pdf/22/15/4182/3949396/2009jcli2392_1.pdf

Balmaseda MA, Mogensen K, Weaver AT (2013) Evaluation of the ECMWF ocean reanalysis system ORAS4. Q J R Meteorol Soc 139(674):1132–1161. https://doi.org/10.1002/qj.2063

Balmaseda M, Hernandez F, Storto A, Palmer M, Alves O, Shi L, Smith G, Toyoda T, Valdivieso M, Barnier B, Behringer D, Boyer T, Chang YS, Chepurin G, Ferry N, Forget G, Fujii Y, Good S, Guinehut S, Haines K, Ishikawa Y, Keeley S, Köhl A, Lee T, Martin M, Masina S, Masuda S, Meyssignac B, Mogensen K, Parent L, Peterson K, Tang Y, Yin Y, Vernieres G, Wang X, Waters J, Wedd R, Wang O, Xue Y, Chevallier M, Lemieux JF, Dupont F, Kuragano T, Kamachi M, Awaji T, Caltabiano A, Wilmer-Becker K, Gaillard F (2015) The Ocean Reanalyses Intercomparison Project (ORA-IP). J Oper Oceanogr 8(sup1):s80–s97. https://doi.org/10.1080/1755876X.2015.1022329

Behringer DW (2007) The global ocean data assimilation system at NCEP. In: 11th symp on integrated observing and assimilation systems for atmosphere, oceans and land surface, pp 14–18

Binet D, Gobert B, Maloueki L (2001) El Niño-like warm events in the Eastern Atlantic (6° N , 20° S) and fish availability from Congo to Angola (1964–1999). Aquat Liv Resour 14(2):99–113. https://doi.org/10.1016/S0990-7440(01)01105-6

Bjerknes J (1969) Atmospheric teleconnections from the equatorial pacific. Mon Weather Rev 97(3):163–172. 10.1175/1520-0493(1969)097<0163:ATFTEP>2.3.CO;2

Brierley C, Wainer I (2018) Inter-annual variability in the tropical atlantic from the last glacial maximum into future climate projections simulated by cmip5/pmip3. Clim Past 14(10):1377–1390. https://doi.org/10.5194/cp-14-1377-2018, https://cp.copernicus.org/articles/14/1377/2018/

Burls NJ, Reason CJC, Penven P, Philander SG (2012) Energetics of the tropical atlantic zonal mode. J Clim 25(21):7442–7466. https://doi.org/10.1175/JCLI-D-11-00602.1, https://journals.ametsoc.org/jcli/article-pdf/25/21/7442/4009172/jcli-d-11-00602_1.pdf

Carton JA, Zhou Z (1997) Annual cycle of sea surface temperature in the Tropical Atlantic Ocean. J Geophys Res Oceans 102(C13):27,813–27,824. https://doi.org/10.1029/97JC02197

Carton JA, Cao X, Giese BS, Silva AMD (1996) Decadal and interannual SST variability in the tropical Atlantic Ocean. J Phys Oceanogr 26(7):1165–1175. 10.1175/1520-0485(1996)026<1165:DAISVI>2.0.CO;2

Carton JA, Chepurin GA, Chen L (2018) SODA3: a new ocean climate reanalysis. J Clim 31(17):6967–6983. https://doi.org/10.1175/JCLI-D-18-0149.1

Chiang JCH, Vimont DJ (2004) Analogous Pacific and Atlantic meridional modes of tropical atmosphere-ocean variability. J Clim 17(21):4143–4158. https://doi.org/10.1175/JCLI4953.1

Deppenmeier AL, Haarsma RJ, Hazeleger W (2016) The Bjerknes feedback in the tropical atlantic in CMIP5 models. Clim Dyn 47(7–8):2691–2707. https://doi.org/10.1007/s00382-016-2992-z

Deser C, Alexander MA, Xie SP, Phillips AS (2010) Sea surface temperature variability: patterns and mechanisms. Annu Rev Mar Sci 2(1):115–143. https://doi.org/10.1146/annurev-marine-120408-151453

Ding H, Keenlyside N, Latif M (2009) Seasonal cycle in the upper equatorial atlantic ocean. J Geophys Res. https://doi.org/10.1029/2009JC005418

Ding H, Keenlyside NS, Latif M (2010) Equatorial Atlantic interannual variability: role of heat content. J Geophys Res Oceans. https://doi.org/10.1029/2010JC006304

Dippe T, Lübbecke J, Greatbatch R (2019) A comparison of the atlantic and pacific bjerknes feedbacks: seasonality, symmetry, and stationarity. J Geophys Res Oceans. https://doi.org/10.1029/2018JC014700

Frankignoul C, Kestenare E (2002) The surface heat flux feedback. Part I: estimates from observations in the Atlantic and the North Pacific. Clim Dyn 19(8):633–647. https://doi.org/10.1007/s00382-002-0252-x

Frankignoul C, Kestenare E, Botzet M, Carril AF, Drange H, Pardaens A, Terray L, Sutton R (2004) An intercomparison between the surface heat flux feedback in five coupled models, COADS and the NCEP reanalysis. Clim Dyn 22(4):373–388. https://doi.org/10.1007/s00382-003-0388-3

Graham FS, Brown JN, Langlais C, Marsland SJ, Wittenberg AT, Holbrook NJ (2014) Effectiveness of the bjerknes stability index in representing ocean dynamics. Clim Dyn 43(9):2399–2414. https://doi.org/10.1007/s00382-014-2062-3

Haarsma RJ, Hazeleger W (2007) Extratropical atmospheric response to equatorial atlantic cold tongue anomalies. J Clim 20(10):2076–2091. https://doi.org/10.1175/JCLI4130.1

Hu ZZ, Kumar A, Ren HL, Wang H, L'Heureux M, Jin FF (2013) Weakened interannual variability in the tropical Pacific Ocean since 2000. J Clim 26(8):2601–2613. https://doi.org/10.1175/JCLI-D-12-00265.1

Illig S, Bachèlery ML (2019) Propagation of subseasonal equatorially-forced coastal trapped waves down to the benguela upwelling system. Sci Rep 9:5306. https://doi.org/10.1038/s41598-019-41847-1

Illig S, Dewitte B, Ayoub N, du Penhoat Y, Reverdin G, De Mey P, Bonjean F, Lagerloef GSE (2004) Interannual long equatorial waves in the tropical atlantic from a high-resolution ocean general circulation model experiment in 1981–2000. J Geophys Res Oceans. https://doi.org/10.1029/2003JC001771

Illig S, Bachèlery ML, Lübbecke JF (2020) Why do benguela niños lead atlantic niños? J Geophys Res Oceans 125(9):e2019JC016003. https://doi.org/10.1029/2019JC016003

Jansen MF, Dommenget D, Keenlyside N (2009) Tropical atmosphere-ocean interactions in a conceptual framework. J Clim 22(3):550–567. https://doi.org/10.1175/2008JCLI2243.1

Jin FF (1997) An equatorial ocean recharge paradigm for ENSO. Part I: conceptual Model Pacific from his analysis of the empirical relations of. J Atmos Sci 54:811–829. 10.1175/1520-0469(1997)054<0811:AEORPF>2.0.CO;2

Jin FF, An SI (1999) Thermocline and zonal advective feedbacks within the equatorial ocean recharge oscillator model for ENSO. Geophys Res Lett 26(19):2989–2992. https://doi.org/10.1029/1999GL002297

Jin FF, Kim ST, Bejarano L (2006) A coupled-stability index for ENSO. Geophys Res Lett 33(23):2–5. https://doi.org/10.1029/2006GL027221

Keenlyside NS, Latif M (2007) Understanding equatorial atlantic interannual variability. J Clim 20(1):131–142. https://doi.org/10.1175/JCLI3992.1

Köhl A (2015) Evaluation of the GECCO2 ocean synthesis: transports of volume, heat and freshwater in the Atlantic. Q J R Meteorol Soc 141(686):166–181. https://doi.org/10.1002/qj.2347

Kucharski F, Bracco A, Yoo JH, Molteni F (2007) Low-frequency variability of the indian monsoon–enso relationship and the tropical atlantic: the "weakening" of the 1980s and 1990s. J Clim 20(16):4255–4266. https://doi.org/10.1175/JCLI4254.1, https://journals.ametsoc.org/jcli/article-pdf/20/16/4255/3937107/jcli4254_1.pdf

Kucharski F, Bracco A, Yoo JH, Molteni F (2008) Atlantic forced component of the indian monsoon interannual variability. Geophys Res Lett. https://doi.org/10.1029/2007GL033037

Kumar BP, Vialard J, Lengaigne M, Murty VS, McPhaden MJ (2012) TropFlux: air-sea fluxes for the global tropical oceans: description and evaluation. Clim Dyn 38(7–8):1521–1543. https://doi.org/10.1007/s00382-011-1115-0. arXiv:1011.1669v3

Lindzen RS, Nigam S (1987) On the role of sea surface temperature gradients in forcing low-level winds and convergence in the tropics. J Atmos Sci 44(17):2418–2436. 10.1175/1520-0469(1987)044<2418:OTROSS>2.0.CO;2,https://journals.ametsoc.org/jas/article-pdf/44/17/2418/3423901/1520-0469(1987)044_2418_otross_2_0_co_2.pdf

Losada T, Rodríguez-Fonseca B, Janicot S, Gervois S, Chauvin F, Ruti P (2010) A multi-model approach to the Atlantic Equatorial Mode: impact on the West African Monsoon. Clim Dyn 35(1):29–43. https://doi.org/10.1007/s00382-009-0625-5

Lübbecke JF, McPhaden MJ (2013) A comparative stability analysis of Atlantic and Pacific Niño Modes. J Clim 26(16):5965–5980. https://doi.org/10.1175/JCLI-D-12-00758.1

Lübbecke JF, McPhaden MJ (2014) Assessing the twenty-first century shift in ENSO variability in terms of the Bjerknes stability index. J Clim 27(7):2577–2587. https://doi.org/10.1175/JCLI-D-13-00438.1

Lübbecke JF, Rodríguez-Fonseca B, Richter I, Martín-Rey M, Losada T, Polo I, Keenlyside NS (2018) Equatorial Atlantic variability—modes, mechanisms, and global teleconnections. WIREs Clim Change 9(4):e527. https://doi.org/10.1002/wcc.527

Maeda S, Urabe Y, Takemura K, Yasuda T, Tanimoto Y (2016) Active role of the itcz and wes feedback in hampering the growth of the expected full-fledged el niño in 2014. SOLA 12:17–21. https://doi.org/10.2151/sola.2016-004

Martín-Rey M, Polo I, Rodríguez-Fonseca B, Losada T, Lazar A (2018) Is there evidence of changes in tropical atlantic variability modes under AMO phases in the observational record? J Clim 31(2):515–536. https://doi.org/10.1175/JCLI-D-16-0459.1

Masuda S, Awaji T, Sugiura N, Matthews JP, Toyoda T, Kawai Y, Doi T, Kouketsu S, Igarashi H, Katsumata K, Uchida H, Kawano T, Fukasawa M (2010) Simulated rapid warming of abyssal north pacific waters. Science 329(5989):319–322. https://doi.org/10.1126/science.1188703

Nnamchi H, Li J, Kucharski F, Kang IS, Keenlyside N, Chang P, Farneti R (2015) Thermodynamic controls of the Atlantic Niño. Nat Commun. https://doi.org/10.1038/ncomms9895

Nnamchi HC, Li J, Kucharski F, Kang IS, Keenlyside NS, Chang P, Farneti R (2016) An equatorial-extratropical dipole structure of the Atlantic Niño. J Clim 29(20):7295–7311. https://doi.org/10.1175/JCLI-D-15-0894.1

Nnamchi HC, Latif M, Keenlyside NS, Park W (2020) A satellite era warming hole in the equatorial Atlantic ocean. J Geophys Res Oceans 125(4):e2019JC015,834. https://doi.org/10.1029/2019JC015834

Okumura Y, Xie SP (2004) Interaction of the Atlantic equatorial cold tongue and the African Monsoon*. J Clim 17(18):3589–3602. 10.1175/1520-0442(2004)017<3589:IOTAEC>2.0.CO;2,https://journals.ametsoc.org/jcli/article-pdf/17/18/3589/3786824/1520-0442(2004)017_3589_iotaec_2_0_co_2.pdf

Prigent A, Lübbecke J, Bayr T, Latif M, Wengel C (2020) Weakened sst variability in the tropical atlantic ocean since 2000. Clim Dyn. https://doi.org/10.1007/s00382-020-05138-0

Prodhomme C, Voldoire A, Exarchou E, Deppenmeier AL, García-Serrano J, Guemas V (2019) How does the seasonal cycle control equatorial Atlantic interannual variability? Geophys Res Lett 46(2):916–922. https://doi.org/10.1029/2018GL080837

Richter I, Xie SP (2008) On the origin of equatorial atlantic biases in coupled general circulation models. Clim Dyn 31:587–598. https://doi.org/10.1007/s00382-008-0364-z

Richter I, Xie SP, Behera S, Doi T, Masumoto Y (2012) Equatorial Atlantic variability and its relation to mean state biases in CMIP5. Clim Dyn. https://doi.org/10.1007/s00382-012-1624-5

Richter I, Behera SK, Masumoto Y, Taguchi B, Sasaki H, Yamagata T (2013) Multiple causes of interannual sea surface temperature variability in the equatorial Atlantic Ocean. Nat Geosci 6(3):43. https://doi.org/10.1038/ngeo1660

Richter I, Xie SP, Behera SK, Doi T, Masumoto Y (2014) Equatorial atlantic variability and its relation to mean state biases in cmip5. Clim Dyn 42(1–2):171–188

Saha S, Moorthi S, Pan HL, Wu X, Wang J, Nadiga S, Tripp P, Kistler R, Woollen J, Behringer D, Liu H, Stokes D, Grumbine R, Gayno G, Wang J, Hou YT, Chuang HY, Juang HMH, Sela J, Iredell M, Treadon R, Kleist D, Van Delst P, Keyser D, Derber J, Ek M, Meng J, Wei H, Yang R, Lord S, Van Den Dool H, Kumar A, Wang W, Long C, Chelliah M, Xue Y, Huang B, Schemm JK, Ebisuzaki W, Lin R, Xie P, Chen M, Zhou S, Higgins W, Zou CZ, Liu Q, Chen Y, Han Y, Cucurull L, Reynolds RW, Rutledge G, Goldberg M (2010) The NCEP climate forecast system reanalysis. Bull Am Meteorol Soc 91(8):1015–1057. https://doi.org/10.1175/2010BAMS3001.1

Servain J, Wainer I, McCreary JP, Dessier A (1999) Relationship between the equatorial and meridional modes of climatic variability in the Tropical Atlantic. Geophys Res Lett 26(4):485–488. https://doi.org/10.1029/1999GL900014

Servain J, Clauzet G, Wainer IC (2003) Modes of Tropical Atlantic climate variability observed by PIRATA. Geophys Res Lett. https://doi.org/10.1029/2002GL015124

Servain J, Caniaux G, Kouadio YK, McPhaden MJ, Araujo M (2014) Recent climatic trends in the Tropical Atlantic. Clim Dyn 43(11):3071–3089. https://doi.org/10.1007/s00382-014-2168-7

Stramma L, Schott F (1999) The mean flow field of the Tropical Atlantic Ocean. Deep Sea Res Part II 46(1):279–303. https://doi.org/10.1016/S0967-0645(98)00109-X

Tokinaga H, Xie SP (2011) Weakening of the Equatorial Atlantic cold tongue over the past six decades. Nat Geosci 4(4):222–226. https://doi.org/10.1038/ngeo1078

Xie SP (1994) On the genesis of the equatorial annual cycle. J Clim 7(12):2008–2013. 10.1175/1520-0442(1994)007<2008:OTGOTE>2.0.CO;2

Xie SP, Carton JA (2013) Tropical Atlantic variability: patterns, mechanisms, and impacts. American Geophysical Union (AGU), pp 121–142. https://doi.org/10.1029/147GM07

Xue Y, Balmaseda MA, Boyer T, Ferry N, Good S, Ishikawa I, Kumar A, Rienecker M, Rosati AJ, Yin Y (2012) A comparative analysis of upper-ocean heat content variability from an ensemble of operational ocean reanalyses. J Clim 25(20):6905–6929. https://doi.org/10.1175/JCLI-D-11-00542.1

Yadav RK, Srinivas G, Chowdary JS (2018) Atlantic Niño modulation of the Indian Summer Monsoon through the Asian Jet. Clim Atmos Sci 1(1):23. https://doi.org/10.1038/s41612-018-0029-5

Yang H, Wang F (2009) Revisiting the thermocline depth in the equatorial Pacific. J Clim 22(13):3856–3863. https://doi.org/10.1175/2009JCLI2836.1

Zebiak SE (1993) Air-sea interaction in the equatorial Atlantic region. J Clim 6(8):1567–1586. 10.1175/1520-0442(1993)006<1567:AIITEA>2.0.CO;2

Zhang S, Harrison MJ, Rosati A, Wittenberg A (2007) System design and evaluation of coupled ensemble data assimilation for global oceanic climate studies. Mon Weather Rev 135(10):3541–3564. https://doi.org/10.1175/MWR3466.1

Zhu J, Huang B, Balmaseda M (2012) An ensemble estimation of the variability of upper-ocean heat content over the Tropical Atlantic Ocean with multi-ocean reanalysis products. Clim Dyn 39:1001–1020. https://doi.org/10.1007/s00382-011-1189-8

Zuidema P, Chang P, Medeiros B, Kirtman BP, Mechoso R, Schneider EK, Toniazzo T, Richter I, Small RJ, Bellomo K, Brandt P, de Szoeke S, Farrar JT, Jung E, Kato S, Li M, Patricola C, Wang Z, Wood R, Xu Z (2017) Challenges and Prospects for Reducing Coupled Climate Model SST Biases in the Eastern Tropical Atlantic and Pacific Oceans: The U.S. CLIVAR Eastern Tropical Oceans Synthesis Working Group. Bulletin of the American Meteorological Society 97(12):2305–2328, https://doi.org/10.1175/BAMS-D-15-00274.1, https://journals.ametsoc.org/bams/article-pdf/97/12/2305/3748158/bams-d-15-00274_1.pdf